

Crossover from interaction to driven regimes in quantum vortex reconnections

Luca Galantucci,^{1,*} A. W. Baggaley,¹ N. G. Parker,¹ and C. F. Barenghi¹

¹*Joint Quantum Centre (JQC) Durham–Newcastle,
and School of Mathematics and Statistics, Newcastle University,
Newcastle upon Tyne, NE1 7RU, United Kingdom*

(Dated: March 6, 2022)

Reconnections of coherent filamentary structures play a key role in the dynamics of fluids, redistributing energy and helicity among the length scales, triggering dissipative effects and inducing fine-scale mixing. Unlike ordinary (classical) fluids where vorticity is a continuous field, in superfluid helium and in atomic Bose-Einstein condensates (BECs) vorticity takes the form of isolated quantised vortex lines, which are conceptually easier to study. New experimental techniques now allow visualisation of individual vortex reconnections in helium and condensates. It has long been suspected that reconnections obey universal laws, particularly a universal scaling with time of the minimum distance between vortices δ . Here we perform a comprehensive analysis of this scaling across a range of scenarios relevant to superfluid helium and trapped condensates, combining our own numerical simulations with the previous results in the literature. We reveal that the scaling exhibit two distinct fundamental regimes: a $\delta \sim t^{1/2}$ scaling arising from the mutual interaction of the reconnecting strands and a $\delta \sim t$ scaling when extrinsic factors drive the individual vortices.

RECONNECTIONS IN CLASSICAL AND QUANTUM SYSTEMS

Reconnections of coherent filamentary structures (Fig. 1) play a fundamental role in the dynamics of plasmas (from astrophysics [1–3] to confined nuclear fusion), nematic liquid crystals [4], polymers and macromolecules [5] (including DNA [6]), optical beams [7, 8], ordinary (classical) fluids [9–11] and quantum fluids [12, 13]. In fluids, the coherent structures consist of concentrated vorticity, whose character depends on the classical or quantum nature of the fluid: in classical fluids (air, water etc.), vorticity is a continuous field and the interacting structures are *vortex tubes* of arbitrary core size around which the circulation of the velocity field is unconstrained; in quantum fluids (atomic Bose-Einstein Condensates (BECs), and superfluid ^4He and ^3He), the structures are isolated one-dimensional *vortex lines*, corresponding to topological defects of the governing order parameter around which the velocity’s circulation is quantized [14–17].

The discrete nature of quantum vortices makes them ideal for the study of vortex reconnections, which assume the form of isolated, dramatic events, strongly localised in space and time. First conjectured by Feynman [15] and then numerically predicted [19], quantum vortex reconnections been observed only recently, both in superfluid ^4He [20] (indirectly, using tracer particles) and in BECs [21] (directly, using an innovative stroboscopic visualisation technique).

Vortex reconnections are crucial in redistributing the kinetic energy of turbulent superfluids. In some regimes, they trigger a turbulent energy cascade [22] in which vortex lines self-organise in bundles [23], generating the same Kolmogorov spectrum of classical turbulence [22, 24–27].

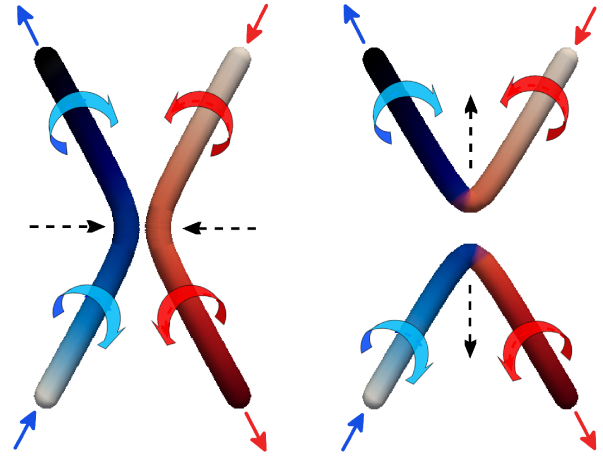


FIG. 1. Reconnecting vortex lines exchanging strands. Schematic vortex configurations before the reconnection (left) and after (right); the vortices’ shape is as determined analytically by Nazarenko and West [18]. Color gradient along the vortices and blue/red arrows indicate the directions of the vorticity along the vortices and the direction of the flow velocity around them. Dashed black arrows indicate the vortex motion, first towards each others, then away from each others.

By altering the topology of the flow [28], reconnections also seem to redistribute its helicity [29, 30], although the precise definition of helicity in superfluids is currently debated [30–32], and the effects of reconnections [33–36] on its geometric ingredients (link, writhe and twist) are still discussed. In the low-temperature limit, losses due to viscosity or mutual friction are negligible, and reconnections are the ultimate mechanism for the dissipation of the incompressible kinetic energy of the superfluid via sound radiation at the reconnecting event [37, 38] followed by further sound emission by the Kelvin wave cas-

cade [39–41] which follows the relaxation of the reconnection cusps.

IS THERE A UNIVERSAL ROUTE TO RECONNECTION ?

Many authors have focused on the possibility that there is a *universal route* to reconnection, which may take the form of a vortex ring cascade [42, 43], a particular rule for the cusp angles [44, 45], or, more promising, a special scaling with time of the minimum distance $\delta(t)$ between the reconnecting vortex strands. It is on the last property that we concentrate our attention.

Several studies have observed a symmetrical pre/post reconnection scaling of $\delta(t)$ [18, 44, 46–48]; others have suggested an asymmetrical scaling possibly ascribed to acoustic energy losses [38, 49, 50], similar to the asymmetry observed in classical Navier-Stokes fluids [51]. In Fig. 2 (top) and (bottom) we present a comprehensive summary of the scaling of $\delta(t)$, combining previous numerical and experimental results with data computed in the present study; this spans an impressive eight orders of magnitude.

The aim of this paper is to reveal that there are *two* distinct fundamental scaling regimes for $\delta(t)$. In addition to the known [18, 44, 46–48, 52–54] $\delta \sim t^{1/2}$ scaling, we predict and observe a new linear scaling $\delta(t) \sim t$. We show how the two scalings arise from rigorous dimensional arguments, then demonstrate them in numerical simulations of vortex reconnections

DIMENSIONAL ANALYSIS

We conjecture that, in the system under consideration (superfluid helium, atomic BECs), δ depends only upon the following physical variables: the time t from the reconnection, the quantum of circulation κ of the superfluid, a characteristic lengthscale ℓ associated to the geometry of the vortex configuration, the fluid’s density ρ , and the density gradient $\nabla\rho$. We hence postulate the following functional form

$$f(\delta, t, \kappa, \ell, \rho, \nabla\rho) = 0. \quad (1)$$

Following the standard procedure of the Buckingham π -theorem [55] (see SI Appendix SI.1 for details), we derive the following scalings:

$$\delta(t) = (C_1\kappa)^{1/2}t^{1/2} \quad \textit{interaction regime}, \quad (2)$$

$$\delta(t) = C_2 \left(\frac{\kappa}{\ell}\right) t \quad \textit{driven regime}, \quad (3)$$

$$\delta(t) = C_3 \left(\kappa \frac{\nabla\rho}{\rho}\right) t \quad \textit{driven regime}, \quad (4)$$

where C_1, C_2 and C_3 are dimensionless constants. Physically, the $\delta \sim t^{1/2}$ scaling of Eq. (2) identifies the quantum of circulation κ as the only relevant parameter driving the reconnection dynamics [20]; this scaling corresponds to a vortex dynamics driven by the mutual interaction between vortex strands, as illustrated more in detail in section A.

Equations (3, 4), on the other hand, introduce the new $\delta \sim t$ scaling. This scaling suggests the presence of a characteristic velocity which drives the approach/separation of the vortex lines. Indeed, we can offer some physical examples of these velocities. If ℓ is the radius of a vortex ring, then $v_\ell = C_2(\kappa/\ell)$ is, to a first approximation, the self-induced velocity of the ring. Alternatively, if ℓ is equal to the distance of a vortex to a sharp boundary in an otherwise homogeneous BEC (such as arises for BEC confined by box traps), then v_ℓ is the self-induced vortex velocity arising from the presence of an image vortex. Finally, if the BEC density is smoothly-varying (such as arises for BECs confined by harmonic traps) then $v_{\nabla\rho} = C_3(\kappa\nabla\rho/\rho)$ is precisely the individual velocity of a vortex induced by the density gradients, C_3 depending on the trap’s geometry [56, 57]. In the next section we will see how these scalings, and the crossover, emerge in typical scenarios through numerical simulations.

NUMERICAL SIMULATIONS

There are two established models of quantum vortex dynamics: the Gross-Pitaevskii (GP) model and the Vortex Filament (VF) method. The former describes a weakly-interacting BEC in the zero-temperature limit [58], the latter is based on the classical Biot-Savart law describing the velocity field of a given vorticity distribution, which in our case is concentrated on space curves [59, 60].

The main difference between GP and VF models is the probed lengthscales of the flow. The GP equation is a *microscopic*, compressible model, capable of describing density fluctuations and lengthscales smaller than the vortex core a_0 (defined as the diameter of the cylindrical tube around the superfluid vortex-line where the density is within 75% of the bulk density). In the GP model, vortices are identified as topological phase defects of the condensate wavefunction Ψ , and reconnections are solutions of the GP equation itself. On the other hand, the VF method is a *mesoscopic* incompressible model, probing the features of the flow at lengthscales much larger than the vortex core, typically $10^4 a_0$ or $10^5 a_0$, neglecting any density perturbation created by moving vortices and the density depletions represented by the vortex cores themselves. In the VF model, vortex lines are discretised employing a set of Lagrangian points whose dynamics is governed by the classical Biot-Savart law, and vortex re-

connections are performed by an *ad hoc* ‘cut-and-paste’ algorithm [59, 61].

In the present study, we employ both GP and VF models to investigate the scaling with time of the minimum distance δ between reconnecting vortices. Technical details of these methods are described in SI Appendix SI.6 and SI.7. Distinctive of our simulations is the larger initial distance δ_0 compared to past numerical studies (5 to 20 times larger in GP simulations, 100 to 2000 larger in VF ones). We also extend the use of the GP model to inhomogeneous, confined BECs where vortex reconstructions can now be investigated experimentally with unprecedented resolution [21].

Homogeneous unbounded systems

To make progress in the understanding of vortex reconstructions in homogenous quantum fluids, we identify two limiting initial vortex configurations which generate the two fundamental types of reconstructions. The first configuration consists of two initially straight and orthogonal vortices, corresponding to the limit where the curvatures K_1 and K_2 of the two vortices are small and comparable (*i.e.* $K_1 \sim K_2$ and $K_1, K_2 \ll 1$); the second configuration is a vortex ring interacting with an isolated vortex line, which is the limiting case of two vortices of significantly different curvatures ($K_1 \ll K_2$ or $K_1 \gg K_2$). The third limiting case of large and comparable curvatures ($K_1 \sim K_2$ and $K_1, K_2 \gg 1$), *i.e.* the collision of small vortex rings, is neglected in the present study as it refers to an extremely unlikely event, due to the small cross section.

The orthogonal reconnection configuration, and the corresponding results for $\delta(t)$, are shown in Fig. 3 (left) and reported in movies S1-S4. Previous GP simulations of this geometry used initial distances $\delta_0 \lesssim 6\xi$, where $\xi = \hbar/\sqrt{2mgn}$ is the healing length of the system ($a_0 \approx 4\xi$ to 5ξ), and m , g and n are the boson mass, the repulsive strength of boson interaction and the bulk density of bosons respectively. Here we extend the investigations to initial distances $\delta_0 \approx 30\xi$. Introducing the rescaled distance $\delta^* = \delta/\xi$ and time $t^* = |t - t_r|/\tau$ (where t_r is the reconnection instant and $\tau = \xi/c$, $c = \sqrt{gn/m}$ being the speed of sound in a homogeneous BEC), we observe that for $\delta^* \lesssim 2.5$ (when the two vortex lines are so close to each other that the condensate’s density in the region between them is significantly less than the bulk density) a symmetrical $t^{*1/2}$ scaling emerges clearly for both pre- and post-reconnection dynamics. This is consistent with the most recent GP simulations [48] and inconsistent with other numerical GP studies [38, 50], adding further evidence to a $t^{*1/2}$ symmetrical scaling at small distances for orthogonal reconstructions.

To map quantitatively the emergence of the $t^{*1/2}$ be-

	$\delta^* < 2.5$	$2.5 < \delta^* < 10$	$\delta^* > 10$
α^-	0.48	0.40	0.43
α^+	0.49	0.60	0.50

TABLE I. **GP simulations: homogeneous unbounded BECs, orthogonal reconnection.** Scaling exponents α^- (α^+) for power law behaviour $\delta^* \sim t^{*\alpha}$ for pre (post) reconnection dynamics for initial separation $\delta_0^* = 20$.

haviour in distinct intervals of δ , in Table I we report the scaling exponents α of the power-law fits $\delta^* \sim t^{*\alpha}$ for the intermediate initial distance $\delta_0^* = 20$. From the table it clearly emerges that the $t^{*1/2}$ scaling also holds in the post-reconnection dynamics at large distances, while in the intermediate region $2.5 < \delta^* < 10$ (both pre- and post reconnection) and at large distances during the approach, the scalings deviate from $t^{*1/2}$. In order to investigate these deviations, we calculate the velocity contribution of the local vortex curvature, v_γ , to the approach/separation velocity $d\delta^*/dt^*$ for the intermediate initial distance $\delta_0^* = 20$, displaying the corresponding results in Fig. 4 (top) (see SI Appendix SI.2 for the calculation of v_γ). The figure clearly shows that the observed deviations from the $t^{*1/2}$ scaling depend on the relative curvature contribution $\sigma = v_\gamma/(d\delta^*/dt^*)$: the larger σ , the more prominent the deviations from the $t^{*1/2}$ behaviour. This implies that the $t^{*1/2}$ scaling observed at large distances in the separation dynamics originates from an interaction-dominated motion of the reconnecting strands. If the dynamics is governed by the mutual interaction of the two vortices, in fact, $d\delta^*/dt^* \propto \kappa/(4\pi\delta^*)$ [44], leading straightforwardly to the scaling $\delta^* \sim t^{*1/2}$, derived in Eq. (2). This argument corroborates the experimentally observed $t^{*1/2}$ scaling [46, 52]. Concluding our study of orthogonal reconstructions, we note that vortex lines move faster after the reconnection than before it, as pointed out in past studies [38, 48–50], and that the post-reconnection curves show a slight sensitivity to the initial distance δ_0^* .

The second homogeneous system which we consider is a vortex ring reconnecting with an isolated initially straight vortex line (see movies S5-S8). This scenario is notably relevant in superfluid helium turbulence at low temperatures, where the low density of thermal excitations is not able to quickly damp out small vortex structures. In fact, the methods used to generate turbulence at low temperatures involve either injecting vortex rings [62–65] or vibrating small structures (*e.g.* spheres, wires and grids) which trigger a great number of ring - line collisions [66–68]. Similarly, also inhomogeneous quantum turbulence [69, 70] and boundary layer turbulence [71] display conspicuous vortex loop - vortex line collisions.

Figure 3 (right) illustrates this vortex set-up and

presents the behaviour of $\delta(t)$. We vary the initial radius of the ring ($R_0^* = R_0/\xi = 5, 7.5$ and 10), while keeping constant its initial distance $\delta_0^* = 100$ to the line. We first focus on the pre-reconnection evolution of $\delta(t)$. This clearly reveals the two distinct scalings predicted by the dimensional analysis:

$$\delta^*(t^*) \sim a_{1/2} t^{*1/2} \quad \text{for } t^* \lesssim 5, \quad (5)$$

$$\delta^*(t^*) \sim a_1 t^* \quad \text{for } t^* \gtrsim 20, \quad (6)$$

where $a_{1/2}$ and a_1 are constant prefactors corresponding, respectively, to $(C_1\kappa)^{1/2}$ in Eq. (2) and v_ℓ or $v_{\nabla\rho}$ in Eqs. (3) or (4). To our knowledge, the linear scaling has not been reported in previous studies. We also note that the crossover between these two regimes occurs at a distance of $\delta_c \sim 3 - 4\xi$; we will revisit the importance of this scale later.

The linear scaling implies that $d\delta^*/dt^*$ is constant: at large distances, the relative velocity between the two points at minimum distance, \mathbf{x}_{ring} (on the vortex ring) and \mathbf{x}_{line} (on the vortex line), projected on the separation vector $\boldsymbol{\delta} = \mathbf{x}_{\text{ring}} - \mathbf{x}_{\text{line}}$, is constant with respect to time. We argue that, at large separation distances $d\delta^*/dt^*$ is approximately equal to the initial speed of the vortex ring [72]:

$$\frac{d\delta^*}{dt^*} = v_{\text{ring}}^* = \frac{\kappa}{4\pi\xi c R_0^*} \left[\ln(8R_0^*) - 0.615 \right]. \quad (7)$$

The self-induced velocity of the vortex ring v_{ring} thus plays the role of the characteristic velocity v_ℓ in Eq. (3). We make the notation compact and rewrite Eq. (7) as $v_{\text{ring}}^* = Cf(\tilde{R}_0)$, where $C = \kappa/(4\pi c \bar{R}_0)$, $f(\tilde{R}_0) = [\ln(\tilde{R}_0) + 3.48]/\tilde{R}_0$, $\bar{R}_0 = 7.5\xi$ is the average radius of the three simulations, and $\tilde{R}_0 = R_0/\bar{R}_0$. We then arrive at the result that Eq. (6) takes the form $\delta^*(t^*) \sim Cf(\tilde{R}_0)t^*$. This is confirmed in Fig. 3 (right, inset): when δ^* is rescaled as $\delta^*/f(\tilde{R}_0)$ the curves collapse onto a single curve in the $\delta \sim t$ regime. The clear $t^{*1/2}$ scaling for $\delta^* \lesssim \delta_c^*$ is consistent with the interpretation put forward for the orthogonal reconnection, as at such small distances, the approach/separation is likely to be governed by the mutual interaction of the two vortices given that δ is smaller than the ring's radius of curvature.

We hence suggest that these two scalings correspond to a crossover from a dynamics predominantly driven by mutual vortex interaction ($\delta^* \sim t^{*1/2}$ scaling) to the self-driven (curvature-driven) motion of the ring ($\delta^* \sim t^*$ scaling). To check this conjecture, we again refer to the contribution of the local vortex curvature: Fig. 4 (bottom) shows the relative curvature contribution for the ring-line pre-reconnection dynamics. We see that the contribution from the local vortex curvature to the approach velocity drops dramatically for $t^* \lesssim 5$, corre-

sponding exactly to the onset of the $t^{*1/2}$ scaling, supporting this picture.

The crossover between the two scalings, however, is less apparent in the post-reconnection dynamics, and for two main reasons. Firstly, both vortices become perturbed by propagating Kelvin-waves; secondly, the travelling velocity of the perturbed vortex ring is not constant [73–75]. These Kelvin waves generate sound waves [76, 77] dissipating the incompressible kinetic energy, leading to a decrease of the length of the vortex ring and a damping of the oscillations' amplitude. When these oscillations die out (*e.g.* in the simulation with $R_0^* = 5$, see Fig. 3 (right)), and the vortex ring regains its circular shape travelling at constant velocity away from the vortex line, we recover the expected $\delta^* \sim t^*$ scaling. This wobbling dynamics and the recovery of the linear scaling are addressed in more detail in SI Appendix SI.3.

The same qualitative behaviour for the orthogonal vortices and ring-line scenario is recovered in VF simulations (see SI Appendix SI.4, Fig. S2). In the latter scenario, the crossover from $t^{*1/2}$ to t^* scaling occurs at much larger lengthscales than in the GP simulations, given the range of scales involved ($\approx 10^5 a_0 - 10^8 a_0$). However, as for GP simulations, the distance δ_c at which the crossover takes place is determined by the balance between interaction-dominated motion and curvature-driven dynamics, *i.e.* by the comparison between $\delta(t)$ and the radius of curvature $R_c(t)$ of the vortex ring.

Trapped systems

Since it is now experimentally possible to visualise individual quantum reconnections in trapped atomic BECs [21, 78], we test the above results under such realistic experimental set-ups. We consider two classes of traps: the widely-employed *harmonic traps* [79] (Figs. 5 and 6 and movies S9 and S10) and the recently-designed *box-traps* [80, 81] (see SI Appendix SI.5 and movies S11 and S12). We employ GP simulations throughout this analysis (the VF model is not suitable for inhomogeneous systems).

In harmonic traps the condensate is inhomogeneous (the density is larger near the centre) and individual motion of the vortices (responsible for the linear scaling) is determined by their curvature, density gradients and, possibly, vortex images [56, 57, 82, 83]. In box-traps the condensate's density is constant (with the exception of a thin layer of width of the order of the healing length near the boundary), and the individual vortex motion is believed to be driven by image vortices with respect to the boundaries, according to two-dimensional studies [84]. We exploit these self-driven vortex motions to analyse reconnections starting from initial distances significantly larger than previous numerical simulations (up to 20 times larger).

Consider first the harmonic trap case; the initial configuration is shown in Fig. 5. The condensate is taken to be cigar-shaped, with the long axis along x (the trapping frequency ω_x along x is smaller than those in the transverse directions, $\omega_y = \omega_z = \omega_\perp$). In this geometry, a single straight vortex line imprinted off center on a radial plane is known to orbit around the center of the condensate [85, 86] along an elliptical orbit perpendicular to itself. The vortex follows a trajectory of constant energy [57] which is uniquely determined by the orbit parameter $\chi = x_0/R_x = r_0/R_\perp$, where x_0 and r_0 are the axial and radial semi-axes of the ellipse, and R_x and R_\perp are the axial and radial Thomas-Fermi radii respectively. The period T of this orbit decreases with increasing χ [57, 78, 83, 87, 88], $T = \frac{8\pi(1-\chi^2)\mu}{3\hbar\omega_\perp\omega_x \ln(R_\perp/\xi_c)}$, where ξ_c is the healing length at the center of the trap. Hence, outer vortices (with larger values of χ) move faster.

If two orthogonal vortices are imprinted on radial planes, intersecting the (long) x axis at opposite positions $\pm x_0$, distinct vortex interactions can occur (vortex rebounds, vortex reconnections, double reconnections, ejections) depending on the value of the orbit parameter χ [21]. Results presented here refer to three different values of χ , all engendering vortex reconnections: $\chi = 0.35, 0.5, 0.6$. The pre-reconnection evolution of $\delta^* = \delta/\xi_c$ is reported in Fig. 6 (left). As for the ring-line reconnection, we observe a cross-over from $t^{*1/2}$ to t^* scaling. This occurs for all values of χ . Moreover, the $t^{*1/2}$ scaling again occurs in the region $\delta^* \lesssim 5$, suggesting that this feature is indeed universal for vortex reconnections in BECs.

If we rescale the minimum distance δ with the healing length ξ_r evaluated at the reconnection point \mathbf{x}_r , $\xi_r = \frac{\hbar}{\sqrt{2gmn_{\text{TF}}(\mathbf{x}_r)}}$ ($n_{\text{TF}}(\mathbf{x}_r)$ being the condensate particle density according to the Thomas-Fermi approximation), the curves corresponding to distinct values of χ overlap for $\delta_r^* = \delta/\xi_r \lesssim 5$ (see the inset of the right panel of Fig. 6). This result implies that ξ_r (hence the radius of the vortex core) is the correct lengthscale which characterises the approach dynamics when vortex cores start merging. Furthermore, the dependence of ξ_r on $mn_{\text{TF}}(\mathbf{x}_r)$ indicates that mass density $\rho = mn$ itself plays a significant role in determining the minimum distance δ - this is exactly why we included ρ in the set of physical variables when applying Buckingham's π -Theorem.

Another similarity between reconnections in harmonic traps and other geometries is the faster post-reconnection dynamics, as seen in the inset of Fig. 6 (left). This velocity difference between approach and separation (related to an increase of the local vortex curvature in the reconnection process and to an emission of acoustic energy) seems a universal feature of quantum vortex reconnections [48] and also observed in simulations of reconnecting classical vortex tubes [51].

Figure 6 (left) shows that $\frac{d\delta^*}{dt^*}$ is constant for $t^* \gtrsim 20$ before the reconnection, increasing with increasing values of the orbital parameter χ (this is not surprising since isolated vortices move faster on outer orbits). It seems reasonable to assume that $\frac{d\delta^*}{dt^*} = Cf(\chi)$, where $f(\chi) = \frac{\chi}{1-\chi^2}$ and C is a constant which depends on the trap's geometry. Indeed, the magnitude of the vortex velocity induced by both density gradients [57, 82, 89] and vortex curvature (assuming, for simplicity, that the shape of the vortex is an arc of a circle) are proportional to $f(\chi)$. As a consequence, we expect that $\delta^*(t^*) \sim Cf(\chi)t^*$ for $t^* \gtrsim 20$. This conjecture is confirmed in Fig. 6 (right): when plotted as $\delta^*/f(\chi)$, the curves for different χ collapse onto a universal curve in this region.

We stress that the observed linear scaling at large distances is a novel result. However, although we have numerically identified the dependence of $d\delta^*/dt^*$ on χ at large distances, we still lack a simple physical justification of this result.

In harmonic traps, the predominant effect driving the approach of the vortices at large distances is hence the individual vortex motion driven by curvature and density gradients (the role of vortex images still remains unclear [83] in this trap geometry), independent of the presence of the other vortex. The scaling crossover in harmonic traps is thus governed by the balance between the interaction of the reconnecting strands and the driving of the individual vortices, as it occurs for the ring - line reconnection in homogeneous BECs described previously.

The nature of this scaling crossover is confirmed by the investigation of vortex reconnections in box-trapped BECs, outlined in SI Appendix SI.5 (see, in particular, Fig. S4). In these trapped systems, the motion of individual vortices is found to be driven by vortex images, leading to a linear scaling at large distances. At small distance we again recover the $\delta \sim t^{*1/2}$ scaling. The results obtained in all the trapped BECs investigated in this work, hence, always show a $\delta \sim t^{*1/2}$ to $\delta \sim t^*$ scaling crossover which, we stress, has not been observed in past studies. In addition, the always observed small scale $\delta \sim t^{*1/2}$ behaviour supports the argument for the existence of a universal scaling law at length scales close to the reconnection point.

The role of density depletions

Current and previous GP simulations of reconnections in homogeneous and trapped BECs, see a clear symmetric pre/post-reconnection $t^{*1/2}$ scaling in the region $\delta^* \lesssim 5$, irrespective of the initial condition. The effect is robust and mostly went unnoticed, as the prefactors $a_{1/2}$ in Eq. (5) may vary depending on the conditions

and between the approach/separation.

Figure 7 shows the condensate density along the line containing the separation vector between two reconnecting vortices (taken to be the ring-line scenario in a homogeneous system), as a function of t^* and the distance $r^* = r/\xi$ to the mid-point of the separation segment. It is clear that for $t^* \lesssim 5$, which is when the $t^{*1/2}$ scaling appears, the density between the two vortices drops dramatically. This behaviour is generic - we obtain it also for any vortex reconnection set-up and across homogeneous and trapped BECs. This result confirms the analytical work of Nazarenko and West [18], who Taylor-expanded the solution of the GP for reconnecting vortex lines and predicted the observed $t^{1/2}$ scaling in this limit of vanishing density (in this limit the cubic nonlinear term vanishes, reducing the GP equation to the linear Schrödinger equation). There are hence two different arguments for the observation of the $t^{1/2}$ scaling: the interaction-driven dynamics argument, underlying the dimensional scaling of Eq. (2), and the vanishing density argument from the GP equation. The arguments are both valid at small lengthscales, consistently with the $t^{1/2}$ scaling observed close to reconnection in all GP simulations.

CONCLUSIONS

We have addressed the question of whether there is a universal route to quantum vortex reconnections by performing an extensive campaign of numerical simulations using the two main mathematical models available (the Gross-Pitaevskii equation and Vortex Filament method). What distinguishes our work from previous studies is that, firstly, we have studied the *two* main physical systems which display quantised vorticity (trapped atomic condensates and superfluid helium), and, secondly, that we have considered the behaviour over distances one order of magnitude larger. By applying rigorous dimensional arguments, we have found that the minimum distance between reconnecting vortex lines may obey two fundamental scaling law regimes: the already observed $\delta^* \sim t^{*1/2}$ scaling and a new $\delta^* \sim t^*$ scaling.

At small lengthscales, we always observe the $\delta^* \sim t^{*1/2}$ scaling; this arises from either the mutual interaction between reconnecting strands or from the depleted density/nonlinearity in the reconnection region. The observation of this scaling in all GP simulations, independently of the precise nature of the system (homogeneous or trapped) and initial vortex configuration, adds further evidence for the existence of this universal $\delta^* \sim t^{*1/2}$ scaling law close to reconnection. At larger lengthscales, two fundamental limiting cases appear: the continuation of the $\delta^* \sim t^{*1/2}$ scaling if the dynamics is still governed by the vortex mutual interaction, or a linear $\delta^* \sim t^*$ behaviour if vortices are individually driven by extrinsic

factors, such as curvature, density gradients and boundaries/images. In the latter case, the crossover between the two scaling regimes is determined by the balance between interaction-dominated motion and individually driven dynamics. This scaling behaviour is summarised schematically in Fig. 8. We stress that these two fundamental scaling laws represent limiting behaviours: intermediate scalings can arise due to additional physics, *e.g.* Kelvin waves. We also stress that the $\delta^* \sim t^*$ cannot arise from a uniform flow, which would simply advect both vortices in the same direction. Instead, it arises in distinct systems, both homogeneous and inhomogeneous, from the different illustrated physical mechanisms, and has not yet been reported in the literature.

While in homogeneous systems the $t^{*1/2}$ behaviour can persist to arbitrary separations (*e.g.* for initially orthogonal and weakly-curved vortices), we find that in trapped condensates the scaling crossover always arises. Indeed, the current technological ability to directly image vortex lines in trapped condensates suggests that full 3D reconstructions will soon be available putting the detection of this crossover within experimental reach.

L.G., C.F.B. and N.G.P. acknowledge the support of the Engineering and Physical Sciences Research Council (Grant No. EP/R005192/1).

* luca.galantucci@newcastle.ac.uk

- [1] Priest E, Forbes T (2007) *Magnetic Reconnection: MHD Theory and Applications*. (Cambridge University Press).
- [2] Che H, Drake J, Swisdak M (2011) A current filamentation mechanism for breaking magnetic field lines during reconnection. *Nature* 474(7350):184.
- [3] Cirtain JW, et al. (2013) Energy release in the solar corona from spatially resolved magnetic braids. *Nature* 493(7433):501–503.
- [4] Chuang I, Durrer R, Turok N, Yurke B (1991) Cosmology in the laboratory: Defect dynamics in liquid crystals. *Science* 251(4999):1336–1342.
- [5] Sumners D (1995) Lifting the curtain: using topology to probe the hidden action of enzymes. *Notices AMS* 42:528.
- [6] Vazques M, Sumners D (2004) Tangles analysis of gin recombination. *Math Pr Cam Ph Soc* 136:565.
- [7] Dennis M, King R, Jack B, O'Holleran K, Padgett M (2010) Isolated optical vortex knots. *Nat Phys* 6:118.
- [8] Berry M, Dennis M (2012) Reconnections of wave vortex lines. *Eur J Phys* 33:723.
- [9] Kida S, Takaoka M (1994) Vortex reconnection. *Annu Rev Fluid Mech* 26(1):169.
- [10] Pumir A, Kerr R (1987) Numerical simulation of interacting vortex tubes. *Phys Rev Lett* 58:1636.
- [11] Kleckner D, Irvine WT (2013) Creation and dynamics of knotted vortices. *Nat Phys* 9(4):253.
- [12] Barenghi C, Donnelly R, Vinen W (2001) *Quantized vortex dynamics and superfluid turbulence*. (Springer).
- [13] Schwarz K (1988) Three-dimensional vortex dynamics in superfluid he4. *Phys Rev B* 38(4):2398.
- [14] Onsager L (1949) Statistical hydrodynamics. *Nuovo Cim*

- 6(Suppl. 2):249.
- [15] Feynmann R (1955) *Application of quantum mechanics to liquid helium*. (N Holland Publ Co) Vol. 1, p. 36.
- [16] Vinen W (1961) The detection of single quanta of circulation in liquid helium ii. *Proc Roy Soc London* 260(1301):218–236.
- [17] Donnelly RJ (1991) *Quantized Vortices in Helium II*. (Cambridge University Press).
- [18] Nazarenko S, West R (2003) Analytical solution for non-linear schrödinger vortex reconnection. *J Low Temp Phys* 132:1.
- [19] Koplik J, Levine H (1993) Vortex reconnection in superfluid helium. *Phys Rev Lett* 71:1375.
- [20] Bewley G, Paoletti M, Sreenivasan K, Lathrop D (2008) Characterization of reconnecting vortices in superfluid helium. *Proc Natl Acad Sci USA* 105:13707.
- [21] Serafini S, et al. (2017) Vortex reconnections and rebounds in trapped atomic bose-einstein condensates. *Phys Rev X* 7:021031.
- [22] Barenghi C, L'vov V, Roche P (2014) Experimental, numerical and analytical velocity spectra in turbulent quantum fluid. *Proc Natl Acad Sci USA* 111(1):supp 1, 4683.
- [23] Baggaley A, Laurie J, Barenghi C (2012) Vortex-density fluctuations, energy spectra, and vortical regions in superfluid turbulence. *Phys Rev Lett* 109:205304.
- [24] Nore C, Abid M, Brachet M (1997) Kolmogorov turbulence in low-temperature superflows. *Phys Rev Lett* 78(20):3896.
- [25] Skrbek L, Sreenivasan K (2012) Developed quantum turbulence and its decay. *Phys Fluids* 24:011301.
- [26] Maurer J, Tabeling P (1998) Local investigation of superfluid turbulence. *Europhys Lett* 43:29.
- [27] Salort J, et al. (2010) Turbulent velocity spectra in superfluid flows. *Phys Fluids* 22:125102.
- [28] Kleckner D, Kauffman L, Irvine W (2016) How superfluid vortex knots untie. *Nat Phys* 12:650.
- [29] Scheeler M, Kleckner D, Proment D, Kindlmann G, Irvine W (2014) Helicity conservation by flow across scales in reconnecting vortex links and knots. *Proc Natl Acad Sci USA* 111:15350.
- [30] Di Leoni P, Mininni PD, Brachet ME (2016) Helicity, topology and kelvin waves in reconnecting quantum knots. *Phys Rev A* 94:043605.
- [31] Salman H (2017) Helicity conservation and twisted seifert surfaces for superfluid vortices. *Proc. R. Soc. A* 473(2200):20160853.
- [32] Barenghi CF, Galantucci L, Parker NG, Baggaley AW (2018) Classical helicity of superfluid helium. *arXiv:1805.09005*.
- [33] Laing C, Ricca R, Sumners D (2015) Conservation of writhe helicity under anti-parallel reconnection. *Sci Rep* 5:9224.
- [34] Zuccher S, Ricca R (2015) Helicity conservation under quantum reconnection of vortex rings. *Phys Rev E* 92(6):061001.
- [35] Zuccher S, Ricca RL (2017) Relaxation of twist helicity in the cascade process of linked quantum vortices. *Phys Rev E* 95(5):053109.
- [36] Hänninen R, Hietala N, Salman H (2016) Helicity within the vortex filament model. *Sci Rep* 6:37571.
- [37] Leadbeater M, Winiecki T, Samuels D, Barenghi C, Adams C (2001) Sound emission due to superfluid vortex reconnections. *Phys Rev Lett* 86(8):1410.
- [38] Zuccher S, Caliarì M, Baggaley A, Barenghi C (2012) Quantum vortex reconnections. *Phys Fluids* 24:125108.
- [39] Kivotides D, Vassilicos J, Samuels D, Barenghi C (2001) Kelvin waves cascade in superfluid turbulence. *Phys Rev Lett* 86:3080.
- [40] Kozik E, Svistunov B (2004) Kelvin-wave cascade and decay of superfluid turbulence. *Phys Rev Lett* 92:035301.
- [41] Kozik E, Svistunov B (2005) Scale-separation scheme for simulating superfluid turbulence: Kelvin-wave cascade. *Phys Rev Lett* 94:025301.
- [42] Kerr R (2011) Vortex stretching as a mechanism for quantum kinetic energy decay. *Phys Rev Lett* 106(22):224501.
- [43] Kurša M, Bajer K, Lipniaki T (2011) Cascade of vortex loops initiated by a single reconnection of quantum vortices. *Phys Rev B* 83:014515.
- [44] De Waele A, Aarts R (1994) Route to vortex reconnection. *Phys Rev Lett* 72(4):482.
- [45] Tebbs R, Youd AJ, Barenghi C (2011) The approach to vortex reconnection. *J Low Temp Phys* 162(3-4):314.
- [46] Paoletti M, Fisher ME, Lathrop D (2010) Reconnection dynamics for quantized vortices. *Physica D: Nonlinear Phenomena* 239(14):1367–1377.
- [47] dos Santos FEA (2016) Hydrodynamics of vortices in bose-einstein condensates: A defect-gauge field approach. *Phys Rev A* 94(6):063633.
- [48] Vilhois A, Proment D, Krstulovic G (2017) Universal and nonuniversal aspects of vortex reconnections in superfluids. *Phys Rev Fluids* 2(4):044701.
- [49] Allen A, et al. (2014) Vortex reconnections in atomic condensates at finite temperature. *Phys Rev A* 90:013601.
- [50] Rorai C, Skipper J, Kerr R, Sreenivasan K (2016) Approach and separation of quantum vortices with balanced cores. *J Fluid Mech* 808:641.
- [51] Hussain F, Duraisamy K (2011) Mechanics of viscous vortex reconnection. *Phys Fluids* 23:021701.
- [52] Fonda E, Sreenivasan K, Lathrop D (2019) Reconnection scaling in quantum fluids. *Proc Nat Acad Sci* 116(6):1924–1928.
- [53] Fonda E, Meichle D, Ouellette N, Hormoz S, Lathrop D (2014) Direct observation of kelvin waves excited by quantized vortex reconnection. *Proc Natl Acad Sci USA* 111(Suppl 1):4707.
- [54] Lipniacki T (2000) Evolution of quantum vortices following reconnection. *Eur J Mech B Fluids* 19(3):361–378.
- [55] Buckingham E (1914) On physically similar systems; illustrations of the use of dimensional equations. *Phys Rev* 4(4):345–376.
- [56] Jackson B, McCann J, Adams C (1999) Vortex line and ring dynamics in a trapped bose-einstein condensate. *Phys Rev A* 61:013604.
- [57] Svidzinsky A, Fetter A (2000) Stability of a vortex in a trapped bose-einstein condensate. *Phys Rev Lett* 84(26):5919.
- [58] Pitaevskii LP, Stringari S (2003) *Bose-Einstein condensation*. (Ox Univ Pr).
- [59] Schwarz K (1985) Three-dimensional vortex dynamics in superfluid he 4: Line-line and line-boundary interactions. *Phys Rev B* 31(9):5782.
- [60] Hänninen R, Baggaley A (2014) Vortex filament method as a tool for computational visualization of quantum turbulence. *Proc Natl Acad Sci USA* p. 201312535.
- [61] Baggaley A (2012) The sensitivity of the vortex filament method to different reconnection models. *J Low Temp Phys* 168(1-2):18–30.

- [62] Walmsley P, Golov A (2008) Quantum and quasiclassical types of superfluid turbulence. *Phys Rev Lett* 100(24):245301.
- [63] Walmsley P, Tompsett P, Zmeev D, Golov A (2014) Reconnections of quantized vortex rings in superfluid he 4 at very low temperatures. *Phys Rev Lett* 113(12):125302.
- [64] Zmeev D, et al. (2015) Dissipation of quasiclassical turbulence in superfluid he 4. *Phys Rev Lett* 115(15):155303.
- [65] Walmsley P, Golov A (2017) Coexistence of quantum and classical flows in quantum turbulence in the $t=0$ limit. *Phys Rev Lett* 118(13):134501.
- [66] Hänninen R, Tsubota M, Vinen W (2007) Generation of turbulence by oscillating structures in superfluid helium at very low temperatures. *Phys Rev B* 75(6):064502.
- [67] Goto R, et al. (2008) Turbulence in boundary flow of superfluid he 4 triggered by free vortex rings. *Phys Rev Lett* 100(4):045301.
- [68] Nakatsuji A, Tsubota M, Yano H (2014) Statistics of vortex loops emitted from quantum turbulence driven by an oscillating sphere. *Phys Rev B* 89(17):174520.
- [69] Nemirovskii SK (2010) Diffusion of inhomogeneous vortex tangle and decay of superfluid turbulence. *Phys Rev B* 81(6):064512.
- [70] Barenghi CF, Samuels DC (2002) Evaporation of a packet of quantized vorticity. *Phys Rev Lett* 89(15):155302.
- [71] Stagg G, Parker N, Barenghi C (2017) Superfluid boundary layer. *Phys Rev Lett* 118(13):135301.
- [72] Roberts PH, Grant J (1971) Motions in a bose condensate. i. the structure of the large circular vortex. *J Phys A: Gen Phys* 4(1):55.
- [73] Arms R, Hama FR (1965) Localized-induction concept on a curved vortex and motion of an elliptic vortex ring. *Phys Fluids* 8(4):553–559.
- [74] Dhanak M, Bernardinis BD (1981) The evolution of an elliptic vortex ring. *J Fluid Mech* 109:189–216.
- [75] Barenghi C, Hänninen R, Tsubota M (2006) Anomalous translational velocity of vortex ring with finite-amplitude kelvin waves. *Phys Rev E* 74(4):046303.
- [76] Kopiev V, Chernyshev S (1997) Vortex ring eigenoscillations as a source of sound. *J Fluid Mech* 341:19–57.
- [77] Parker N, Proukakis N, Barenghi C, Adams C (2004) Controlled vortex-sound interactions in atomic bose-einstein condensates. *Phys Rev Lett* 92(16):160403.
- [78] Serafini S, et al. (2015) Dynamics and interaction of vortex lines in an elongated bose-einstein condensate. *Phys Rev Lett* 115(17):170402.
- [79] Dalfovo F, Giorgini S, Pitaevskii LP, Stringari S (1999) Theory of bose-einstein condensation in trapped gases. *Rev Mod. Phys* 71(3):463.
- [80] Gaunt A, Schmidutz T, Gotlibovych I, Smith, R P.Hadzibabic Z (2013) Bose-einstein condensation of atoms in a uniform potential. *Phys Rev Lett* 110:200406.
- [81] Navon N, Gaunt A, Smith, R P.Hadzibabic Z (2016) Emergence of a turbulent cascade in a quantum gas. *Nature* 539:72.
- [82] Fetter A, Svidzinsky A (2001) Vortices in a trapped dilute bose-einstein condensate. *J. Phys.: Condens. Matter* 13:R135.
- [83] Fetter A (2009) Rotating trapped bose-einstein condensates. *Rev Mod Phys* 81(2):647.
- [84] Mason P, Berloff N, Fetter A (2006) Motion of a vortex line near the boundary of a semi-infinite uniform condensate. *Phys Rev A* 74:043611.
- [85] Anderson B, Haljan P, Wieman C, Cornell E (2000) Vortex precession in bose-einstein condensates: Observations with filled and empty cores. *Phys Rev Lett* 85:2857.
- [86] Freilich D, Bianchi D, Kaufman AM, Langin T, Hall D (2010) Real-time dynamics of single vortex lines and vortex dipoles in a bose-einstein condensate. *Science* 329:1182.
- [87] Lundh E, Ao P (2000) Hydrodynamic approach to vortex lifetimes in trapped bose condensates. *Phys Rev A* 61(6):063612.
- [88] Sheehy D, Radzihovsky L (2004) Vortices in spatially inhomogeneous superfluids. *Phys Rev A* 70:063620.
- [89] Svidzinsky A, Fetter A (2000) Dynamics of a vortex in a trapped bose-einstein condensate. *Phys Rev A* 62:063617.

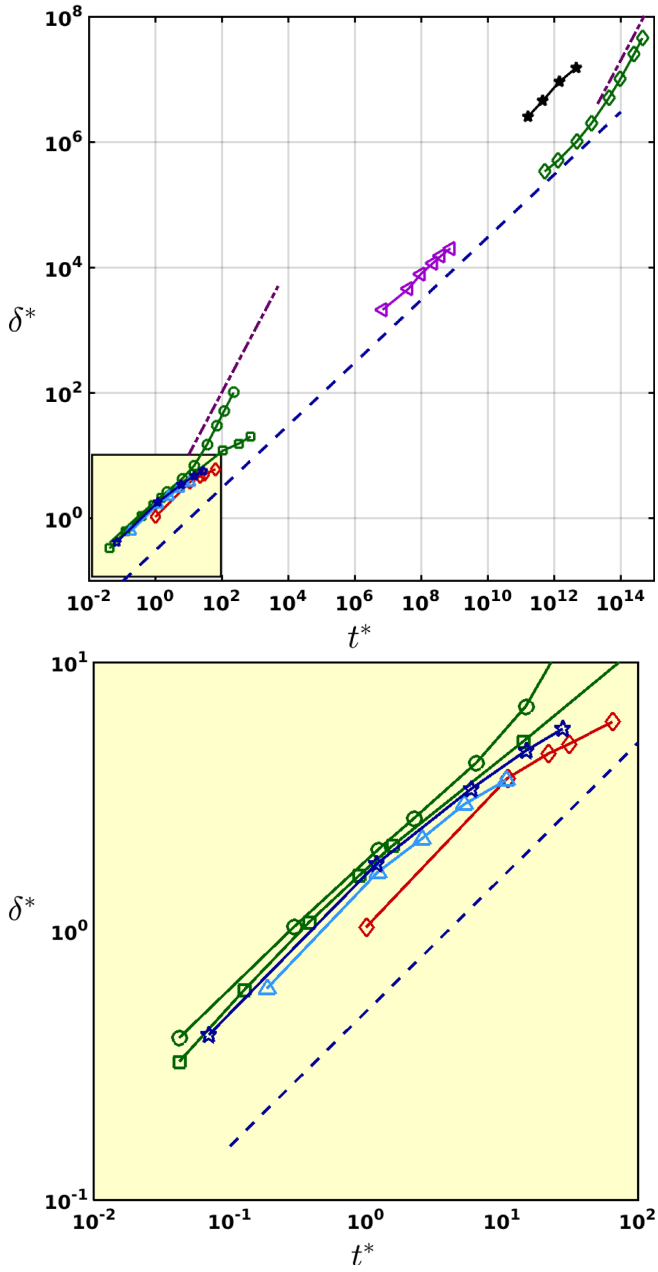


FIG. 2. **Minimum distance between reconnecting vortices: past and present results.** (top): All data reported describe the behaviour of the rescaled minimum distance δ^* between vortices as a function of the rescaled temporal distance to the reconnection event t^* . Empty (filled) symbols refer to pre (post) - reconnection dynamics. **GP simulations:** \diamond Ref. [50]; \star Ref. [48]; \triangle Ref. [38]; \circ and \square , present simulations, ring-vortex collision and orthogonal reconnection, respectively. **VFM simulations:** \blacktriangleleft Ref. [44]; \blacklozenge present simulations, ring-line collision. **Experiments:** \star Ref. [52]. (bottom): zoom on GP simulations.

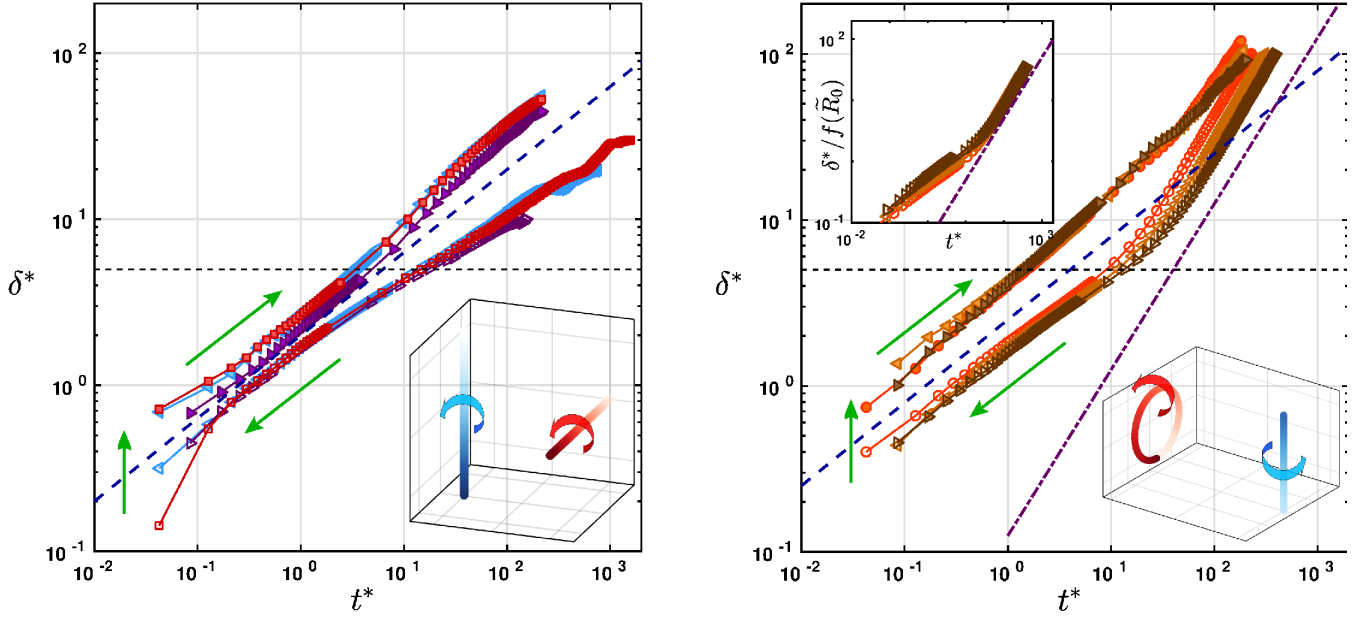


FIG. 3. **GP simulations: homogeneous unbounded BECs.** Evolution of the rescaled minimum distance δ^* between reconnecting vortices as a function of the rescaled temporal distance to reconnection t^* . Empty (filled) symbols correspond to pre (post) reconnection dynamics. **Left:** orthogonal vortices reconnection with rescaled initial distance δ_0^* equal to 10 (\blacktriangleright), 20 (\blacktriangleleft) and 30 (\blacksquare). **Right:** ring-line reconnection for constant initial distance $\delta_0^* = 100$ and vortex ring radii R_0^* equal to 5 (\circ), 7.5 (\triangleleft) and 10 (\blacktriangleright). **Inset:** pre-reconnection dynamics only, the distance is rescaled with $f(\hat{R}_0)$. In both sub figures: the horizontal dashed black line indicates the width of the vortex core ($\approx 5\xi$), the blue-dashed line shows the $t^{*1/2}$ scaling and the bottom insets show the initial vortex configuration. Color gradient on vortices indicates direction of the superfluid vorticity (from light to dark). Dot-dashed violet line in the right panel indicates the t^* scaling. Green arrows indicate the direction of time.

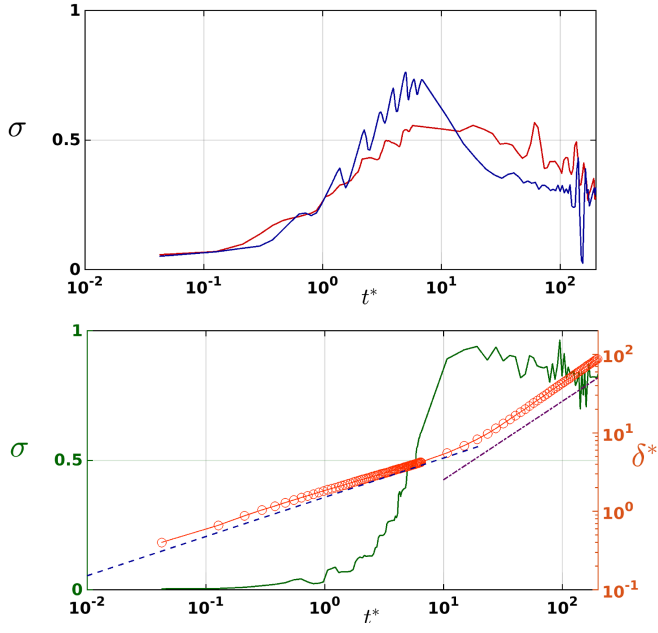


FIG. 4. **Curvature contribution.** (Top): Temporal evolution of the ratio σ for the orthogonal reconnection with initial separation distance $\delta_0^* = 20$; red (blue) symbols correspond to pre (post) reconnection dynamics. (Bottom): Temporal evolution of σ (green solid line) and rescaled minimum distance δ^* (orange circles) for the ring-line pre-reconnection, with $R_0^* = 5$. The blue-dashed line shows the $t^{*1/2}$ scaling, while dot-dashed violet line indicates the t^* scaling.

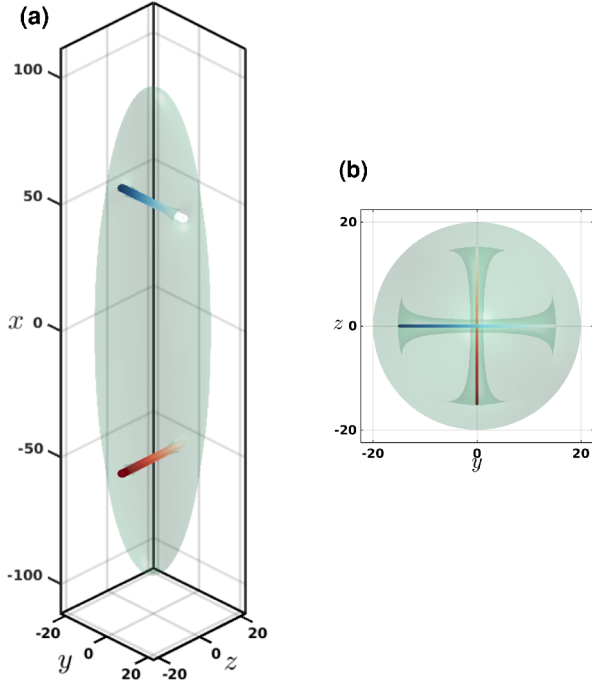


FIG. 5. **GP simulations: harmonically trapped BECs, initial conditions.** (a), (b): Lateral and top view of initial vortex configuration. Light green surfaces are isosurfaces of condensate density at 5% of trap-center density. Color gradient on vortices indicates the direction of the superfluid vorticity (from light to dark). Unit of length is the healing length ξ_c evaluated in the center of the trap.

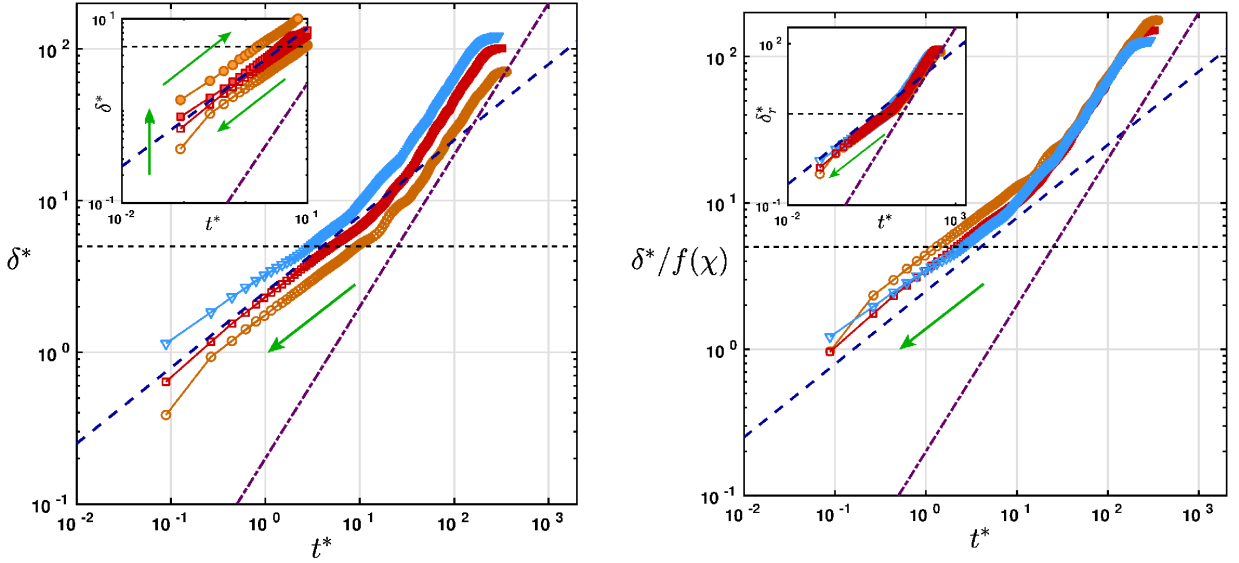


FIG. 6. **GP simulations: harmonically trapped BECs.** Evolution of the minimum distance δ^* between reconnecting vortices as a function of the temporal distance to reconnection t^* . Open (filled) symbols correspond to pre (post) reconnection dynamics. **Left:** pre-reconnection scaling of δ^* for initially imprinted orthogonal vortices with corresponding orbit parameter $\chi = 0.35$ (\circ), $\chi = 0.5$ (\square) and $\chi = 0.6$ (∇). Inset: short-time pre-(open symbols) and post-(filled symbols) reconnection scaling of δ^* for $\chi = 0.35$ (\circ), and $\chi = 0.5$ (\square). **Right:** temporal evolution of the minimum distance δ^* rescaled with $f(\chi)$. Symbols as in left panel. Inset: short-time pre-reconnection scaling of rescaled minimum distance $\delta_r^* = \delta/\xi_r$. In both subfigures, the dashed blue and dot-dashed violet lines show the $t^{*1/2}$ and t^* scalings, respectively. The horizontal dashed line indicates the width of the vortex core at the center of the trap ($\approx 5\xi$). Green arrows indicate the direction of time.

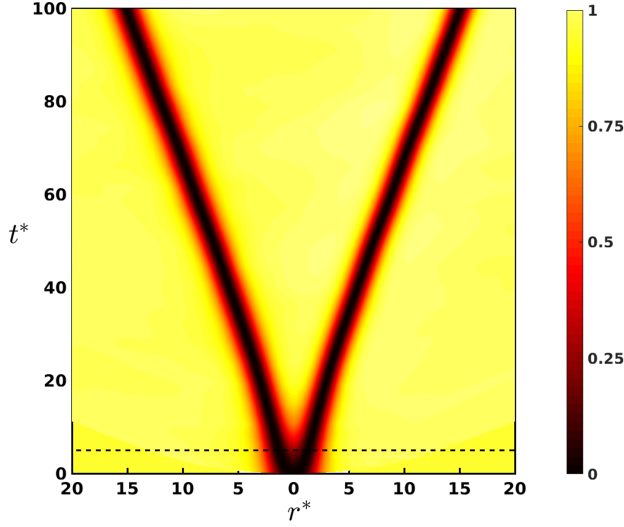


FIG. 7. **The role of density depletions.** Plot of the condensate density along the line containing the separation vector δ between the colliding vortices, as a function of the distance r^* to the mid-point of the separation segment and the rescaled temporal distance to reconnection t^* , for the vortex ring - vortex line pre-reconnection dynamics with $R_0^* = 5$. In the initial phase of the approach (top part of the figure), $\delta \sim t^*$; the cross-over to the $\delta \sim t^{*1/2}$ scaling occurs when the vortex cores start to merge (bottom part) for $t^* \lesssim 5$ (dashed line).

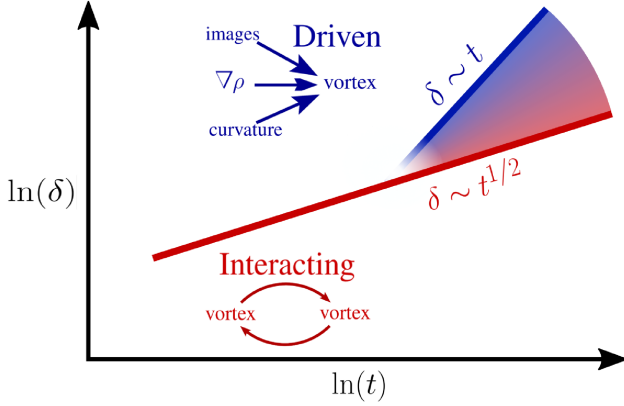


FIG. 8. **Fundamental scalings for the reconnection of two vortex lines.** At small lengthscales the $\delta^* \sim t^{*1/2}$ scaling (in red) is observed as the dynamics is determined by the mutual interaction of the two reconnecting vortex strands. This scaling appears to be universal. At larger distances, we observe two fundamental limiting scenarios: if the motion is still predominantly driven by the interaction, the $\delta^* \sim t^{*1/2}$ scaling (in red) still holds; if the dynamics is governed by extrinsic factors driving the individual vortices a linear $\delta^* \sim t^*$ behaviour is established (in blue). In this last case, a scaling crossover occurs. At large distances, intermediate scalings can arise due to additional physics, *e.g.* Kelvin waves (in red-blue color gradient).

Crossover from interaction to driven regimes in quantum vortex reconnections

Luca Galantucci,^{1,*} A. W. Baggaley,¹ N. G. Parker,¹ and C. F. Barenghi¹

¹*Joint Quantum Centre (JQC) Durham–Newcastle,
and School of Mathematics and Statistics, Newcastle University,
Newcastle upon Tyne, NE1 7RU, United Kingdom*
(Dated: March 6, 2022)

Supporting Information

SI.1: DIMENSIONAL ANALYSIS

In the main text, we conjectured that the minimum distance δ between reconnecting vortex lines depends upon the temporal distance t to reconnection, the quantum of circulation κ , a characteristic lengthscale ℓ associated to the geometry of the vortex configuration, the density ρ and the density gradient $\nabla\rho$, postulating the existence of a functional relation f such that

$$f(\delta, t, \kappa, \ell, \rho, \nabla\rho) = 0. \quad (1)$$

Following the Buckingham π -Theorem [1], there are only three independent dimensionless quantities, π_1 , π_2 and π_3 , which we choose as: $\pi_1 = \delta^2/(\kappa t)$, $\pi_2 = \ell\delta/(\kappa t)$ and $\pi_3 = \rho\delta/(\kappa t\nabla\rho)$. Other dimensionless quantities can be assembled from the same physical variables, but they would depend on π_1 , π_2 and π_3 .

Equation (1) can be rewritten as $\pi_1 = F_1(\pi_2, \pi_3)$, or, equivalently, as $\pi_2 = F_2(\pi_1, \pi_3)$, or as $\pi_3 = F_3(\pi_1, \pi_2)$. Choosing $F_1(\pi_2, \pi_3) = C_1$, $F_2(\pi_1, \pi_3) = C_2$ and $F_3(\pi_1, \pi_2) = C_3$ where C_1 , C_2 and C_3 are constant, we find the scalings reported in the main text, namely

$$\delta(t) = (C_1\kappa)^{1/2}t^{1/2}, \quad (2)$$

$$\delta(t) = C_2 \left(\frac{\kappa}{\ell}\right) t \quad \text{and} \quad (3)$$

$$\delta(t) = C_3 \left(\kappa \frac{\nabla\rho}{\rho}\right) t, \quad (4)$$

where C_1 , C_2 and C_3 are non-dimensional constants. We conclude that there are two distinct scalings: $\delta \sim t^{1/2}$ and $\delta \sim t$.

SI.2: CURVATURE CONTRIBUTION

To find the velocity contribution v_γ arising from the local vortex curvature to the relative approach velocity of the reconnecting vortex lines, $d\delta^*/dt^*$, we proceed as follows. First we compute the velocities $\mathbf{v}_{\gamma,1}$ and $\mathbf{v}_{\gamma,2}$ arising from local vortex curvature of the two points \mathbf{x}_1 and

\mathbf{x}_2 corresponding to the minimum distance. We assume that each velocity can be approximated by the velocity of a circular vortex ring [2] of radius R_c corresponding to the local curvature $K = 1/R_c$ of that vortex strand, which is obtained by taking suitable derivatives with respect to arc length:

$$\mathbf{v}_{\gamma,i} = \frac{\kappa}{4\pi R_{c,i}} \left[\ln\left(\frac{8R_{c,i}}{\xi}\right) - 0.615 \right] \hat{\mathbf{b}}, \quad (5)$$

where $\hat{\mathbf{b}}$ is the unit binormal vector. Secondly, we project $(\mathbf{v}_{\gamma,2} - \mathbf{v}_{\gamma,1})$ on the separation vector $\boldsymbol{\delta} = \mathbf{x}_2 - \mathbf{x}_1$, obtaining $v_\gamma = (\mathbf{v}_{\gamma,2} - \mathbf{v}_{\gamma,1}) \cdot \hat{\boldsymbol{\delta}}$. In order not to overestimate the curvature-driven velocity in the orthogonal reconnection where for most of the simulated dynamics the curvature K is very small ($K = 0$ at the start of simulation), in the calculation of \mathbf{v}_γ for the orthogonal configuration (Fig. 4 (top) main manuscript) we omit the logarithmic correction in Eq. (5).

SI.3: HOMOGENEOUS UNBOUNDED SYSTEMS. GP SIMULATIONS. RING - LINE RECONNECTION.

In this paragraph, we illustrate in more detail the separation (post-reconnection) dynamics of a vortex-ring - vortex-line reconnection occurring in a homogeneous BEC, investigated via GP simulations in the main manuscript (Fig. 3 (right)). The aim is to account for the late recovery of the linear t^{*1} scaling of the minimum distance δ^* . As described in the main text, the linear scaling is observed when (a) the dynamics is governed by the individual motion of the vortices and (b) the projection of the relative velocity on the separation vector $\boldsymbol{\delta}$ is constant with respect to time. In the ring - line reconnections investigated in the present work, the reconnection generates a Kelvin-wave perturbed vortex-line and a non-planar quasi-elliptical vortex-ring (hereafter with 'ring' we intend more generically a closed vortex curve). Due to the presence of these Kelvin waves on the ring, the ring wobbles, and consequently its separation velocity is *not* constant with respect to time [3, 4], explaining the non observation of the scaling crossover $t^{*1/2}$ to t^{*1} as

soon as the vortex cores separate. The wobbling vortex-ring generates sound waves transforming incompressible kinetic energy of the vortex ring in acoustic (compressible) kinetic energy, decreasing the length of vortex lines (which, in the first approximation, is proportional to the incompressible kinetic energy).

The oscillation dynamics of the vortex-ring is illustrated in Fig. S1, where we have reported the temporal evolution of the maximum, minimum and average semi-axes of the vortex-ring, after the reconnection with the vortex-line. As the closed vortex curve is neither a planar curve or perfectly symmetrical, with ‘semi-axes’ we intend the distance of the points $\mathbf{x}(\zeta)$ lying on the vortex curve (where ζ is arclength) from the vortex geometric centre $\mathbf{x}_G = \oint_{\text{ring}} \mathbf{x}(\zeta) d\zeta / \oint_{\text{ring}} d\zeta$.

Figure S1 (left) clearly illustrates that in the simulation with initial vortex-ring radius $R_0^* = 5$, the oscillation becomes negligible for $t^* \gtrsim 50$ where the vortex recovers a circular shape hence travelling at a constant velocity. For $t^* \gtrsim 50$ we indeed recover the linear scaling $\delta^*(t^*) \sim t^*$ (Fig. 3 (right) in main manuscript). In contrast, in the simulation with initial radius $R_0^* = 10$, at $t^* \approx 200$ the vortex-ring is still wobbling (Fig. S1 (right)) explaining why for these initial conditions the linear scaling is not (so far) recovered.

The recovery of the t^{*1} scaling at large distances in the post-reconnection dynamics confers to the ring - line configuration a broad relevance in the context of quantum vortex reconnections, as it highlights its limiting character.

SI.4: VFM SIMULATIONS

Numerical simulations performed using the VFM (Vortex Filament Method) provide further evidence for the scaling laws presented in our article. The VFM [5] applies very well to vortex dynamics in superfluid helium turbulence because of the large separation of scales typical of such problem: $D \gg \ell_v \gg a_0$, where D is the size of the system, ℓ_v the average intervortex distance, and a_0 the vortex core size. When using the VFM to study reconnections of quantum vortices [6]), we must make the following important caveats. Firstly, the VFM does not give information about lengthscales of the order of or smaller than $\Delta\zeta$, defined as the spatial discretisation along the vortex lines; typically, $\Delta\zeta/a_0 \gtrsim 10^5$. Secondly, in the VFM, the motion of vortex line elements is governed by the Biot-Savart law, which formulates the classical Euler equation in integral form. Since vortex reconnections are outside the realm of Euler dynamics, an ad-hoc artificial *cut and paste* algorithm must be implemented [7] (see Methods for further details). Because of the presence of the reconnections algorithm, the VFM cannot provide physical information at lengthscales smaller than $2\Delta\zeta$ or $3\Delta\zeta$.

Still, information about the minimum vortex distance $\delta(t)$ obtained by the VFM at lengthscales larger than $\Delta\zeta$ is important and supports our arguments. In Fig. S2 (left), we report the scaling of δ for initially orthogonal vortices, separated by an initial distance $\delta_0^* = \delta_0/a_0 = 2.5 \times 10^6$. For both pre/post-reconnection dynamics, we only observe the $t^{*1/2}$ scaling, as expected, as the motion of the vortex lines is governed by their mutual interaction.

Fig. S2 (right) illustrates the temporal evolution of δ^* for a ring - line reconnection, and clearly shows the scaling cross-over (arising from the balance between interaction and self-driven motions) which we observe in the corresponding GP simulations. The cross-over takes place when $\delta(t) \lesssim R_c(t)$, $R_c(t)$ being the radius of curvature of the ring in the point \mathbf{x}_{ring} which at time t is at minimum distance from the vortex - line. When $\delta(t) \lesssim R_c(t)$, in fact, the mutual interaction is predominant tending hence towards the $t^{*1/2}$ scaling. The smaller cross-over scale with respect to the initial vortex ring radius R_0 arises from the increasing curvature of the ring while travelling towards the line as an effect of their interaction, *e.g.* at $t_{cr}^* \approx 10^{13}$, in the cross-over region, $R_c^*(t_{cr}^*) \approx 4 \times 10^6$ (while $\delta^*(t_{cr}^*) \approx 2 \times 10^6$).

It is also important to note that in the VF method, the spatial discretisation $\Delta\zeta$ on the vortices constrains the smallest radius of curvature $R_{c,min} \sim 5\Delta\zeta$ which can numerically be resolved. As a consequence, for $\delta \lesssim R_{c,min}$ the scaling will always tend to $t^{*1/2}$.

This $t^{*1/2}$ to t^{*1} crossover in the ring - line reconnection is best recognized in the pre-reconnection stage

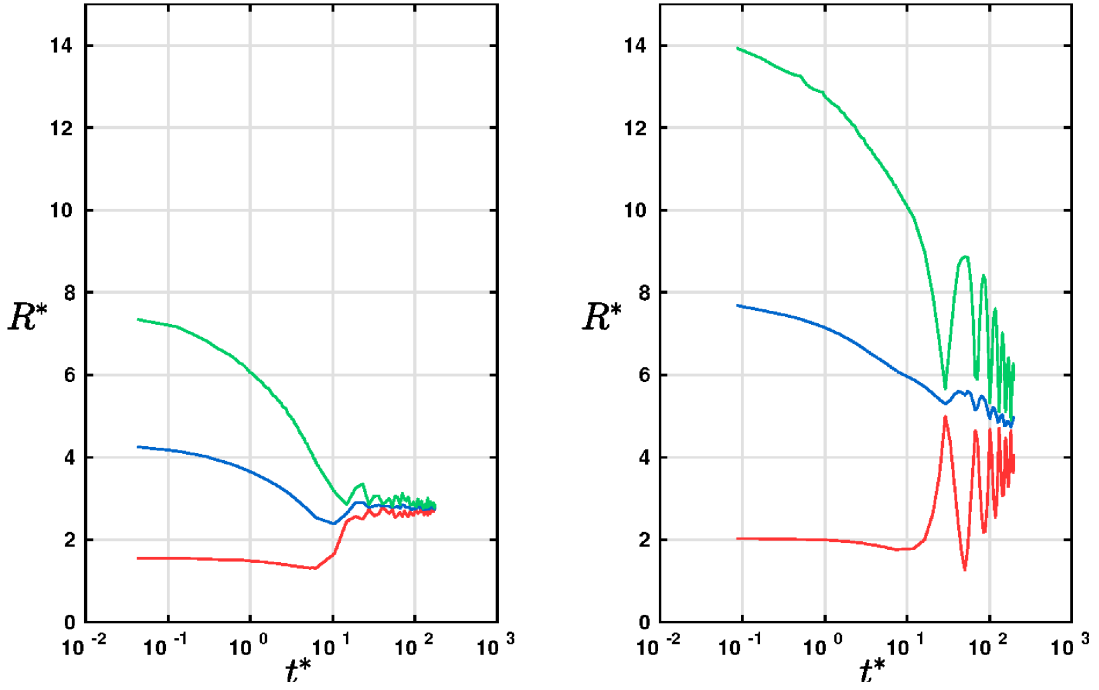


FIG. S1. **GP simulations: post reconnection vortex-ring wobbling.** Post-reconnection temporal evolution of maximum (solid green line), minimum (solid red line) and average (solid blue line) semiaxes R of the vortex-ring produced by the ring-line reconnection described in Fig. 3 (right) of main manuscript. **Left:** initial vortex-ring radius $R_0^* = 5$. **Right:** initial vortex-ring radius $R_0^* = 10$.

(green open symbols) in Fig. S2 (right), where the curve smoothly changes slope. The interpretation of the post-reconnection behaviour (cyan filled symbols) is complicated by the role played by Kelvin waves which are excited by the reconnection event and modify the motions of the line and ring. The scaling exponent is exactly $1/2$ for $2.5 \times 10^{11} \lesssim t^* \lesssim 5 \times 10^{12}$, but we cannot directly ascribe this as being to the mutual interaction of vortices due to the unclear impact of the Kelvin waves.

Movies S13 - S16 show the orthogonal and ring - line reconnections performed with the VFM.

SI.5: BOX-TRAPPED BECS. GP SIMULATIONS

In order to study the scaling of the minimum distance δ with respect to time in further experimentally accessible geometries and with the objective of backing our interpretation of the scaling crossover outlined in the main text, we perform numerical simulations of vortex dynamics and reconnections in recently designed *box-traps* [8, 9]. The fundamental differences between box-trapped BECs and harmonically trapped BECs (investigated in the main text, see Figs. 5 and 6) are mainly two. First, in box-traps the density of the confined BEC is constant throughout the sample (exception made for a thin layer near the trap edges whose width is of the order of the healing length), while in harmonically trapped BECs the condensate density is maximum in the center of the trap and decreases parabolically when moving towards the boundaries of the trap. Second, while the role of images in both box- and harmonically trapped BECs still remains an open question [10–14], in box-traps vortex images with respect to boundaries are believed to be the only source of vortex motion[13]; on the contrary, in harmonic traps vortex dynamics is also determined by density gradients (arising from the inhomogeneous trapping potential) and vortex curvature [10, 15, 16].

The initial vortex configuration for the two simulations performed in box-traps is illustrated in Fig. S3 (a), (b). The initial distance from the top/bottom boundary

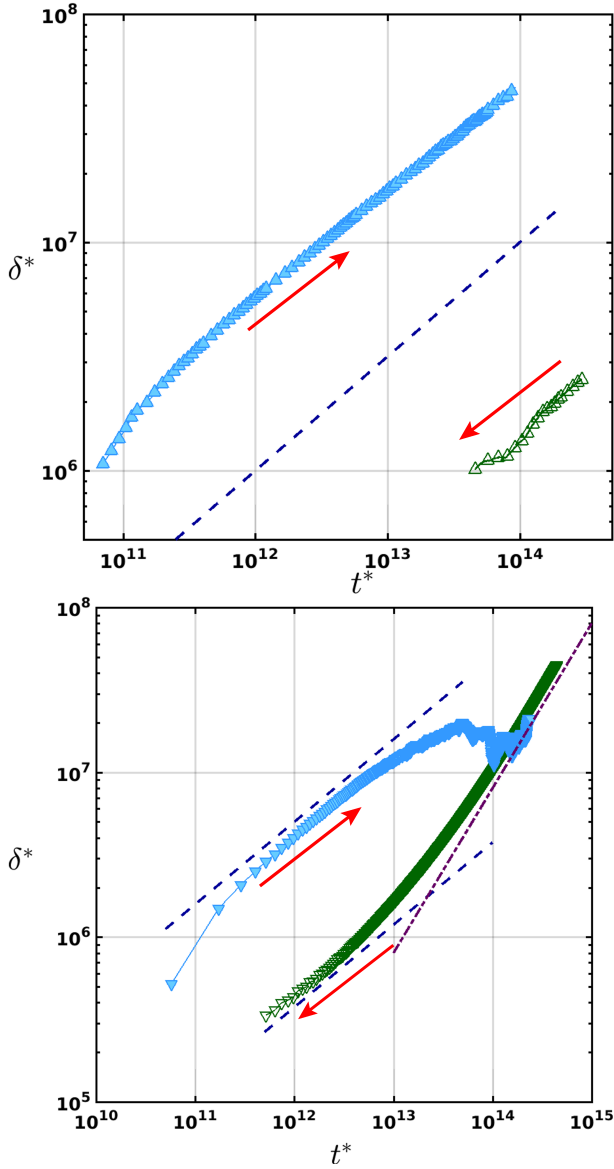


FIG. S2. VFM simulations: homogeneous, unbounded and incompressible superfluid ^4He systems. Evolution of the minimum distance δ^* between reconnecting vortices as a function of the temporal distance to reconnection t^* . Open green (filled cyan) symbols correspond to pre (post) reconnection dynamics. **Left:** reconnection between initially orthogonal vortices with initial distance $\delta_0^* = 2.5 \times 10^6$. **Right:** vortex-ring - vortex-line reconnection for initial distance $\delta_0^* = 4.5 \times 10^7$ and vortex-ring initial radius $R_0^* = 4.2 \times 10^7$. In both subfigures, the blue-dashed line shows the $t^{*1/2}$ scaling. The dot-dashed violet line in the right panel indicates the t^* scaling. Red arrows indicate the direction of time.

$h_0^* = h_0/\xi = 20$ is constant for both simulations (where ξ is the healing length evaluated in the bulk of the condensate, *i.e.* away from the trap boundaries), while to investigate the potential role of images we choose two distinct values of d_0^* : $d_0^* = 8.25$ (dark yellow squares in Fig. S4) and $d_0^* = 11.05$ (red circles in Fig. S4). The

temporal evolution of the minimum distance $\delta^* = \delta/\xi$ is reported in Fig. S4 (left). It clearly emerges that for $t^* \lesssim 10$, δ^* follows a $t^{*1/2}$ scaling indicating that when vortex cores start merging, the predominant dynamics driving the approach of the vortices is the interaction between the latter, consistently with the characteristics of vortex reconnections observed in homogeneous condensates (see Fig. 3 in main manuscript).

In addition, for $t^* \gtrsim 200$ in the approach dynamics, we again observe a linear scaling, *i.e.* $\delta^*(t^*) \sim a_1 t^*$, as in homogeneous BECs (see Fig. 3 in main manuscript), implying a constant value of $d\delta^*/dt^*$. In the present geometry, we conjecture that this constant projection of the relative velocity between vortices on the separation vector (*i.e.* $d\delta^*/dt^*$) coincides with the sum of the velocity magnitudes induced by the vortex images [13],

$$\begin{aligned} \frac{d\delta^*}{dt^*} &= |\mathbf{v}_2 - \mathbf{v}_1| = v_{2,img}^* + v_{1,img}^* \\ &= \frac{\kappa}{2\pi c(d_0 - \sqrt{2}\xi)} = \frac{\kappa}{2\pi c\bar{d}_0} \left[\frac{1}{\tilde{d}_0 - \frac{\sqrt{2}}{d_0^*}} \right] \\ &= C f(\tilde{d}_0) , \end{aligned} \quad (6)$$

where: \mathbf{v}_1 (\mathbf{v}_2) is the velocity of the top (bottom) vortex; $v_{1,img}$ ($v_{2,img}$) is the velocity of the top (bottom) vortex induced by the corresponding image with respect to the lateral boundary of the trap at a distance d_0 (cfr. Fig. S3 (a), (b)); $\tilde{d}_0 = d_0/\bar{d}_0$, $\bar{d}_0 = 9.65\xi$ being the average distance to the lateral boundary of the trap amongst the two simulations performed in box-traps; ξ is the healing length based on the bulk density $n = \mu/g$, with μ and g being the chemical potential and the repulsive interaction strength, respectively; $c = \sqrt{gn/m}$ is the speed of sound; $C = \frac{\kappa}{2\pi c\bar{d}_0}$ is a non-dimensional constant independent

of d_0 and $f(\tilde{d}_0) = \left[\tilde{d}_0 - \frac{\sqrt{2}}{d_0^*} \right]^{-1}$ is a non-dimensional function depending on the distance d_0 .

Hence, for $t^* \gtrsim 200$ in pre-reconnection dynamics we argue that $\delta^*(t^*) \sim C f(\tilde{d}_0) t^*$. This conjecture is confirmed in Fig. S4 (right) where we report the temporal evolution of the rescaled minimum distance $\delta^*/f(\tilde{d}_0)$ for $d_0^* = 8.25$ and $d_0^* = 11.05$: the curves do indeed overlap at large distances. This results confirms, for the first time in literature, that quantum vortices, when confined in three-dimensional box-trapped condensates, are definitely driven by their images with respect to the boundaries of the condensate. The post-reconnection dynamics is less straightforward to investigate as a result of other factors playing a significant role in determining the vortex dynamics, above all acoustic emission and vortex pinning on the boundaries of the trap (as it can

be observed in movies M4).

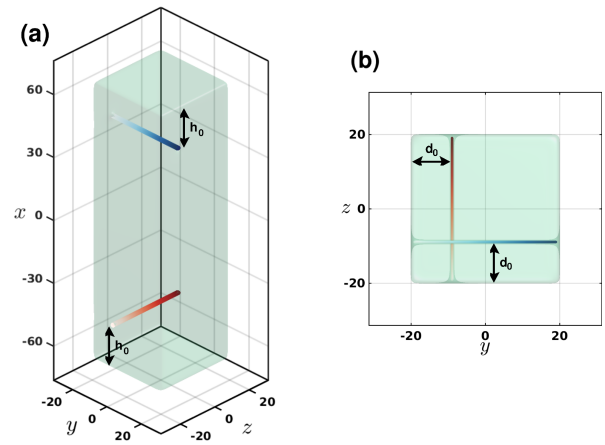


FIG. S3. GP simulations: box-trapped BECs, initial conditions. (a), (b): Lateral and top view of initial vortex configuration for box trapped BECs; Light green surfaces coincide with isosurfaces of condensate density at 5% of trap-center density. Color gradient on vortices indicates the direction of the superfluid vorticity (from light to dark). Unit of length is the healing length ξ evaluated in the bulk of the condensate.

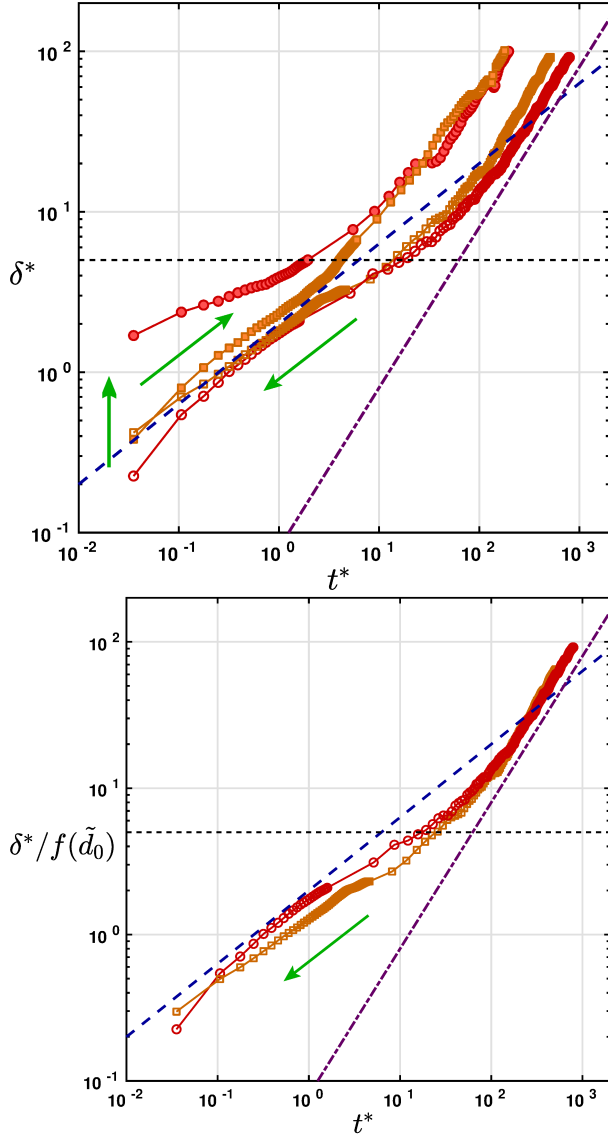


FIG. S4. **GP simulations: box trapped BECs.** Evolution of the minimum distance δ^* between reconnecting vortices as a function of the temporal distance to reconnection t^* . Open (filled) symbols correspond to pre (post) reconnection dynamics. **Left:** pre- and post-reconnection scaling of δ^* for initially imprinted orthogonal vortices at distance \tilde{d}_0^* from trap lateral boundaries and h_0^* from top/bottom boundaries (see Fig.S3): $d_0^* = 8.25$ (\square), $d^* = 11.05$ (\circ); $h_0^* = 20$ for both simulations. **Right:** pre-reconnection scaling of rescaled minimum distance $\delta^*/f(\tilde{d}_0)$. Symbols as in left panel. In both subfigures, the dashed blue and dot-dashed violet lines show the $t^{1/2}$ and t^* scalings, respectively. The horizontal black dashed line indicates the width of the vortex core ($\approx 5\xi$). Green arrows indicate the direction of time.

METHODS

SI.6: Numerical methods for GP simulations

Real-time dynamical simulations of vortex dynamics in BECs at temperature $T = 0$ are performed by numerically integrating the mean-field Gross-Pitaevskii (GP) equation,

$$i\hbar \frac{\partial \Psi}{\partial t} = -\frac{\hbar^2}{2m} \nabla^2 \Psi + V\Psi + g|\Psi|^2\Psi \quad (7)$$

for the complex macroscopic wave function $\Psi(x, y, z, t)$, where m is the boson mass, V is the external potential and $g = 4\pi\hbar^2 a_s/m$ is the strength of the repulsive two-body interaction, a_s being the atomic scattering length.

Our code uses second-order accurate finite differences in space and a fourth order Runge–Kutta method in time.

The algorithm for vortex tracking is based on the pseudo-vorticity unit vector

$$\hat{\omega} := \frac{\nabla\Psi_{\Re} \times \nabla\Psi_{\Im}}{|\nabla\Psi_{\Re} \times \nabla\Psi_{\Im}|}$$

which is tangent to the vortex line along its length [17, 18], where $\Psi = \Psi_{\Re} + i\Psi_{\Im}$.

Homogeneous BECs. In homogeneous systems, the external potential V is zero and the wave function Ψ is normalized by $\Psi_0 = \sqrt{n}$, where $n = \mu/g$ is the homogeneous density of an unbounded BEC in its ground state. By writing $\Psi^* = \Psi/\Psi_0$ and introducing the healing length $\xi = \hbar/\sqrt{2mgn}$ as the unit of length and $\tau = \xi/c$ as the unit of time, where $c = \sqrt{gn/m}$ is the velocity of sound, we obtain the following non-dimensional GP equation:

$$i \frac{\partial \Psi^*}{\partial t^*} = -\frac{1}{2} \nabla^{*2} \Psi^* + \frac{1}{2} |\Psi^*|^2 \Psi^* \quad (8)$$

where the superscript ‘*’ indicates non-dimensional variables. Hereafter all the quantities mentioned are dimensionless, unless otherwise stated, and the superscript ‘*’ is omitted to ease notation.

Orthogonal vortices. We imprint two orthogonal vortices employing Padé approximants [19] for the density field and letting the system evolve in imaginary time: the first is oriented in the negative z direction, the second in the negative y direction. The vortices intersect the x axis at $(-x_0, 0, 0)$ and $(x_0, 0, 0)$ respectively. We compare runs with $x_0 = 5, 10, 15$ leading to initial distances $\delta_0 = 10, 20, 30$ (see the bottom inset in Fig. 3 (left) of the main manuscript). Spatial and time discretization use steps $\Delta x = \Delta y = \Delta z = 0.35$ and $\Delta t = 0.02$. The number of grid-points in the x , y and z direction are $\{N_x, N_y, N_z\} = \{400, 400, 400\}$

respectively, leading to a computational box $\{[x_{\min} : x_{\max}] \times [y_{\min} : y_{\max}] \times [z_{\min} : z_{\max}]\} = \{[-70 : 70] \times [-70 : 70] \times [-70 : 70]\}$.

Ring - line reconnection. We perform simulations for a vortex ring of radius $R_0 = 5, 7.5$ and 10 , and centre $(x_0, y_0, z_0) = (-100, 21, 0)$ on a plane perpendicular to the x direction. The line is oriented in the positive z direction and intersects the y axis at $(x_1, y_1, z_1) = (0, 21, 0)$, as shown in the bottom inset of Fig. 3 (right) in the main manuscript.

The spatial and temporal resolution coincides with orthogonal vortices simulations. The numbers of grid-points in the x , y and z directions are $N_x = 800$, $N_y = 280$ and $N_z = 160$ respectively, leading to a larger computational box: $-140 \leq x \leq 140$, $-50 \leq y \leq 50$ and $-28 \leq z \leq 28$.

Trapped BECs. For harmonically trapped, cigar-shaped BECs the units of length, time and energy are $\ell_{tr} = \sqrt{\hbar/(m\omega_{\perp})}$, $\tau = \omega_{\perp}^{-1}$ and $\epsilon = \hbar\omega_{\perp}$, respectively, where ω_{\perp} is the radial trapping frequency of the harmonic potential. The resulting non-dimensional GP equations is

$$i \frac{\partial \tilde{\Psi}}{\partial \tilde{t}} = -\frac{1}{2} \tilde{\nabla}^2 \tilde{\Psi} + \tilde{V} \tilde{\Psi} + \tilde{g} |\tilde{\Psi}|^2 \tilde{\Psi} \quad (9)$$

where with $\tilde{\cdot}$ we indicate non-dimensional quantities, $\tilde{\Psi}$ is normalized to unity ($\int_V |\tilde{\Psi}|^2 dV = 1$ where V is the volume), and $\tilde{g} = 4\pi N a_s / \ell_{tr}$ and N is the number of atoms in the condensates. Hereafter all the quantities which we mention are meant to be dimensionless unless otherwise stated, and the superscript $\tilde{\cdot}$ is omitted to ease notation.

Box Traps. We choose $g = 2.35 \times 10^4$ and set the trapping potential to

$$V = \begin{cases} 0 & \text{for } |x| < L_x/2 \text{ and } |y| < L_y/2 \text{ and } |z| < L_z/2 \\ 10\mu & \text{elsewhere} \end{cases} \quad (10)$$

where $\mu = 10$ is the chemical potential, $L_x = 29.46\ell_{tr} = 131.75\xi$ and $L_y = L_z = 8.944\ell_{tr} = 40\xi$, ξ being the healing length in the bulk of the condensate.

In Fig. S3 (a), (b), the distance of vortices from the top/bottom edge of the trap is $h_0 = 4.48\ell_{tr} = 20\xi$, leading to the initial minimum distance between vortices $\delta_0 = 20.5\ell_{tr} = 91.75\xi$. The distance of the vortices from the lateral edges is $d_0 = 1.48\ell_{tr} = 8.25\xi$ and $d_0 = 2.47\ell_{tr} = 11.05\xi$. The top vortex is oriented in positive y direction and the bottom vortex is the positive z direction.

The grid-spacings are homogeneous in the three Cartesian directions, $\Delta x = \Delta y = \Delta z = 7.5 \times 10^{-2}$, and

the time step is $\Delta t = 1.25 \times 10^{-3}$. The numbers of grid-points in the x , y and z directions are $N_x = 512$, $N_y = 192$ and $N_z = 192$, leading to the computational box $-19.2 \leq x \leq 19.2$, $-7.2 \leq y \leq 7.2$ and $-7.2 \leq z \leq 7.2$.

Harmonic Traps. We choose $g = 7.4 \times 10^3$ and $\mu = 10$. The trapping potential is

$$V = \frac{1}{2} \left[\left(\frac{\omega_x}{\omega_{\perp}} \right)^2 x^2 + r_{\perp}^2 \right] \quad (11)$$

where $\omega_x = 2\pi \times 26$ Hz is the axial trapping frequency, $\omega_{\perp} = \omega_y = \omega_z = 2\pi \times 131$ Hz is the radial trapping frequency, and $r_{\perp} = (y^2 + z^2)^{1/2}$ is the distance from the axis of the condensate. These parameters correspond to $R_{\perp}/\xi_c = 2\mu/(\hbar\omega_{\perp}) = 20$, where R_{\perp} is the radial Thomas-Fermi radius and ξ_c is the healing length evaluated in the center of the trap.

We imprint two orthogonal vortices as shown in Fig. 5 of main text employing Padé approximants [19] for the density field and letting the system evolve in imaginary time; the top vortex is oriented in the negative y direction, the bottom in the negative z direction. The vortices intersect the x axis at $(\pm x_0, 0, 0)$, where $x_0 = \chi R_x$, $\chi = 0.35, 0.5, 0.6$ is the orbit parameter, and R_x is the axial Thomas-Fermi radius.

Spatial and temporal resolutions coincide with the box-trap simulations. The numbers of grid-points in the x , y and z directions are $N_x = 800$, $N_y = 224$ and $N_z = 224$, leading to the computational box $-30 \leq x \leq 30$, $-8.4 \leq y \leq 8.4$, and $-8, 4 \leq z \leq 8.4$.

SI.7: Numerical methods for VF simulations

The Vortex Filament method [5, 20] is a well-established model widely employed for the numerical simulations of superfluid helium quantum turbulence. A typical superfluid helium experiment is characterised by the large separation of scales between the large scale D of the flow ($D \approx 10^{-2}$ m) and the small length scale of the average inter-vortex distance $\ell_v \approx 10^{-5}$ m; the vortex core radius, $a_0 \approx 10^{-10}$ m in ^4He and about 100 times larger in $^3\text{He-B}$, is even smaller. It is therefore appropriate to mathematically model quantum vortices as closed space curves of infinitesimal thickness $\mathbf{s}(\zeta, t)$, where ζ is arclength and t time, moving in an inviscid Euler fluid according to the BiotSavart law [21, 22],

$$\frac{\partial \mathbf{s}}{\partial t} = \frac{\kappa}{4\pi} \oint_{\mathcal{L}} \frac{\mathbf{s}'(\eta, t) \times [\mathbf{s}(\zeta, t) - \mathbf{s}(\eta, t)]}{|\mathbf{s}(\zeta, t) - \mathbf{s}(\eta, t)|^3} d\eta \quad (12)$$

where the line integration is performed along the entire vortex configuration \mathcal{L} and $\mathbf{s}'(\zeta, t) = \frac{\partial \mathbf{s}}{\partial \zeta}$ is the unit tangent vector.

Vortex-lines are discretised in sets of points $\mathbf{s}_i(t) = \mathbf{s}(\zeta_i, t)$, $i = 1 \dots N$, with initial spatial discretisation $\Delta\zeta = 5 \times 10^{-5}\text{m}$ for the orthogonal reconnection and $\Delta\zeta = 2.5 \times 10^{-5}\text{m}$ for the ring - line reconnection. The Lagrangian dynamics of the vortex points is hence obtained evaluating the discretised Biot-Savart integral starting from a given initial vortex configuration. The singularity of the Biot-Savart integral for $\eta \rightarrow \zeta$ is fixed by taking into account the finite size of the vortex core, yielding [3, 21] the following decomposition between local and non-local contributions:

$$\begin{aligned} \frac{\partial \mathbf{s}}{\partial t} = & \frac{\kappa}{4\pi} \mathbf{s}'(\zeta) \times \mathbf{s}''(\zeta) \ln \left(\frac{2\sqrt{l_+ l_-}}{e^{1/2} a_0} \right) + \\ & + \frac{\kappa}{4\pi} \oint_{\mathcal{L}'} \frac{\mathbf{s}'(\eta) \times [\mathbf{s}(\zeta) - \mathbf{s}(\eta)]}{|\mathbf{s}(\zeta) - \mathbf{s}(\eta)|^3} d\eta, \end{aligned} \quad (13)$$

where time dependence has been omitted to ease notation, \mathbf{s}'' is the normal vector at $\mathbf{s}(\zeta)$ ($|\mathbf{s}''| = K$, K being the curvature at $\mathbf{s}(\zeta)$), l_{\pm} are the lengths of the line segments connected to $\mathbf{s}(\zeta)$ after discretisation, and the integral is evaluated on \mathcal{L}' , the original vortex configuration \mathcal{L} without the line segments adjacent to $\mathbf{s}(\zeta)$.

Reconnections are not intrinsically predicted by the VF method, as Euler inviscid dynamics forbids such changes of topology. As a consequence, an additional algorithm has to be employed which changes the topology of the vortex configuration when two vortex lines become closer than an arbitrary threshold distance which in this work we set to $\Delta\zeta/2$. Moreover, in order to model the dissipative nature (phonon emission) of reconnecting events [23], the numerical *cut and paste* reconnection algorithm reduces vortex length (which is taken as a proxy for the kinetic energy of the vortices). It is important to stress, in fact, that given the length scales of the flow investigated (much larger than the characteristic length-scale of density variations in superfluid helium), the VF method is an incompressible model. Several reconnection algorithms have been introduced in VF method literature. Importantly, a recent analysis [7] has showed that all these algorithms produce very similar results, at least in the context of superfluid turbulence.

The number of discretization points, N , changes with time as the simulation progresses (discretization points are introduced or removed to maintain the numerical resolution along the vortex filaments.) In the present study, if the separation between two discretization points becomes greater than $\Delta\zeta$, a new intermediate point is inserted with the constraint of preserving the vortex curvature. Similarly, if the separation becomes less than $\Delta\zeta/2$, points are removed in order to ensure that our shortest scale which is numerically resolved does not change [24].

In the present work, time integration is performed employing a third order Runge-Kutta method with time

step $\Delta t = 5 \times 10^{-4}\text{s}$, while all spatial derivatives are approximated using fourth-order finite difference schemes which account for varying mesh sizes along the vortex filaments [24, 25].

Movies

Movies S1 - S4

Movies S1, S2, S3 and S4 are a rendering of the reconnection of orthogonal vortices with initial minimum distance $\delta_0^* = 10$, computed employing the Gross-Pitaevskii (GP) model.

Movies S5 - S8

Movies S5, S6, S7 and S8 are a rendering of the reconnection between a vortex ring and a vortex line with initial minimum distance $\delta_0^* = 100$ and initial vortex ring radius $R_0^* = 5$, computed employing the GP model.

Movies S9, S10

Movies S9 and S10 are a rendering of the reconnection between vortex lines in a harmonically trapped Bose-Einstein condensate corresponding to an orbit parameter $\chi = 0.35$, computed employing the GP model.

Movies S11, S12

Movies S11 and S12 are a rendering of the reconnection between vortex lines in a box-trapped Bose-Einstein condensate corresponding to an initial lateral distance from the trap boundary $d_0^* = 11.05$, computed employing the GP model.

Movies S13, S14

Movies S13 and S14 are a rendering of the reconnection of orthogonal vortices with initial minimum distance $\delta_0^* = 2.5 \times 10^6$, computed employing the Vortex Filament (VF) method.

Movies S15, S16

Movies S15 and S16 are a rendering of the reconnection between a vortex ring and a vortex line with initial minimum distance $\delta_0^* = 2 \times 10^7$ and initial vortex ring radius $R_0^* = 1.2 \times 10^7$, computed employing the VF method.

* luca.galantucci@newcastle.ac.uk

- [1] Buckingham E (1914) On physically similar systems; illustrations of the use of dimensional equations. *Phys Rev* 4(4):345–376.
- [2] Roberts PH, Grant J (1971) Motions in a bose condensate. i. the structure of the large circular vortex. *J Phys A: Gen Phys* 4(1):55.
- [3] Arms R, Hama FR (1965) Localized-induction concept on a curved vortex and motion of an elliptic vortex ring. *Phys Fluids* 8(4):553–559.
- [4] Dhanak M, Bernardinis BD (1981) The evolution of an elliptic vortex ring. *J Fluid Mech* 109:189–216.
- [5] Hänninen R, Baggaley A (2014) Vortex filament method as a tool for computational visualization of quantum turbulence. *Proc Natl Acad Sci USA* p. 201312535.
- [6] De Waele A, Aarts R (1994) Route to vortex reconnection. *Phys Rev Lett* 72(4):482.
- [7] Baggaley A (2012) The sensitivity of the vortex filament method to different reconnection models. *J Low Temp Phys* 168(1-2):18–30.
- [8] Gaunt A, Schmidutz T, Gotlibovych I, Smith, R P.Hadzibabic Z (2013) Bose-einstein condensation of atoms in a uniform potential. *Phys Rev Lett* 110:200406.
- [9] Navon N, Gaunt A, Smith, R P.Hadzibabic Z (2016) Emergence of a turbulent cascade in a quantum gas. *Nature* 539:72.
- [10] Fetter A, Svidzinsky A (2001) Vortices in a trapped dilute bose-einstein condensate. *J. Phys.: Condens. Matter* 13:R135.
- [11] Anglin J (2002) Vortices near surfaces of bose-einstein condensates. *Phys Rev A* 65(6):063611.
- [12] Khawaja UA (2005) Vortex dynamics near the surface of a bose-einstein condensate. *Phys Rev A* 71:063611.
- [13] Mason P, Berloff N, Fetter A (2006) Motion of a vortex line near the boundary of a semi-infinite uniform condensate. *Phys Rev A* 74:043611.
- [14] Fetter A (2009) Rotating trapped bose-einstein condensates. *Rev Mod Phys* 81(2):647.
- [15] Svidzinsky A, Fetter A (2000) Stability of a vortex in a trapped bose-einstein condensate. *Phys Rev Lett* 84(26):5919.
- [16] Jackson B, McCann J, Adams C (1999) Vortex line and ring dynamics in a trapped bose-einstein condensate. *Phys Rev A* 61:013604.
- [17] Rorai C, Skipper J, Kerr R, Sreenivasan K (2016) Approach and separation of quantum vortices with balanced cores. *J Fluid Mech* 808:641.
- [18] Vilhois A, Proment D, Krstulovic G (2017) Universal and nonuniversal aspects of vortex reconnections in superfluids. *Phys Rev Fluids* 2(4):044701.
- [19] Berloff N (2004) Padé approximations of solitary wave solutions of the gross-pitaevskii equation. *Journal of Physics A: Mathematical and General* 37(5):1617.
- [20] Schwarz K (1988) Three-dimensional vortex dynamics in superfluid he4. *Phys Rev B* 38(4):2398.
- [21] Schwarz K (1985) Three-dimensional vortex dynamics in superfluid he 4: Line-line and line-boundary interactions. *Phys Rev B* 31(9):5782.
- [22] Saffman P (1992) *Vortex dynamics*. (Cambridge University Press).
- [23] Leadbeater M, Winiecki T, Samuels D, Barenghi C, Adams C (2001) Sound emission due to superfluid vortex reconnections. *Phys Rev Lett* 86(8):1410.
- [24] Baggaley AW, Barenghi CF (2011) Spectrum of turbulent kelvin-waves cascade in superfluid helium. *Phys Rev B* 83:134509.
- [25] Gamet L, Ducros F, Nicoud F, Poinso T (1999) Compact finite difference schemes on non-uniform meshes. application to direct numerical simulations of compressible flows. *Int J Num Meth Fluids* 29(2):159–191.